developed an EIA kit detecting serum IgA antibody specific for GPL core and investigated its usefulness in a multicenter study.

METHODS

See the online supplement for additional methodologic details.

Patients and Serum Samples

Six institutions participated in this study. Between June 2003 and December 2005, serum samples were collected from 70 patients with MAC-PD, 18 with MAC contamination, 36 with pulmonary TB, 45 with other lung diseases, and 76 healthy subjects. All patients with MAC-PD met the ATS guidelines (1). Of the 70 patients with MAC-PD, 64 had previously received combination chemotherapy for mycobacterial diseases recommended by the ATS guidelines, but had MAC-positive cultures at the time of serum collection. Pulmonary TB was confirmed by culture positivity for *M. tuberculosis*. Patients with pulmonary TB who had an underlying pulmonary disease or past history of treatment for pulmonary TB were excluded. Individuals with MAC contamination showed a single culture positive for MAC in small amounts, but were asymptomatic and had no significant chest computed tomography (CCT) findings indicating active mycobacterial disease. The other lung diseases included chronic obstructive pulmonary disease (n = 15), idiopathic interstitial pneumonia (n = 11), lung cancer (n = 11), bacterial pneumonia (n = 4), pulmonary sarcoidosis (n = 2), and bronchiectasis (n = 2). All sera were stored at −20°C until assayed for IgA GPL core antibody. None of the patients was seropositive for HIV type 1 or 2. The patients with MAC-PD were classified into two groups on the basis of the chest radiography: fibrocavitary disease and nodular-bronchiectatic (NBE) disease (1).

Fibrocavitary disease was defined as the presence of cavitary forms in upper lobes. NBE disease was defined as the presence of bronchiectasis and multiple nodular shadows on CCT. Disease conforming to neither of these types was considered unclassifiable. Forty-five patients underwent CCT and serodiagnosis at the same time. A correlation between the extent of disease and antibody levels was investigated. The extent of disease was expressed as the number of MAC-involved CCT segments, as described in the previous study (9).

The studies in human subjects were approved by the research and ethical committees of the NHO National Toneyama Hospital, and written, informed consent was obtained from all subjects.

EIA Kit

The EIA kit was developed by Tauns Laboratories, Inc. (Shizuoka, Japan), with a slight modification of the method described previously (8). Results are given as arbitrary U/ml in relation to a standard curve that was constructed by mixing sera from three patients with MAC-PD as a reference. The intra- and interplate coefficients of variation were 2.27–9.29% and 0.57–8.86%, respectively, which indicated good reproducibility. The linearity of measurement was confirmed. The influence of blood elements and temperature was examined, and revealed good stability. The assay was performed by a technologist with no prior knowledge of the clinical data.

Statistical Analysis

All statistical analyses were performed using GraphPad Prism version 4 (GraphPad Software, Inc., San Diego, CA). Antibody levels in patient groups are expressed as means ± SD. For comparison of the mean values of multiple groups, data were compared by analysis of variance and nonparametric analysis. A probability value of less than 0.05 was regarded as significant.

RESULTS

Study Subjects

The characteristics of the subjects are shown in Table 1. Patients with pulmonary TB and healthy subjects were younger than patients with MAC-PD ($P < 0.001$), and there was a larger proportion of females in the latter group ($P < 0.001$). Of the 70 patients with MAC-PD, 15 had underlying pulmonary disease, all of which were the sequelae of pulmonary TB. Of the 18 individuals with MAC contamination, 15 had underlying pulmonary diseases (8 patients with the sequelae of pulmonary TB, 2 with lung cancer, 2 with chronic obstructive pulmonary disease, 1 with emphysema, 1 with pneumoconiosis, and 1 with sarcoidosis. Of the patients with MAC-PD, 19 were classified as having fibrocavitary disease, and 35 as having NBE disease, with 16 patients unclassifiable. The MAC-PD group included infections with *M. avium* (n = 56), *Mycobacterium intracellulare* (n = 12), or both (n = 2). The MAC contamination group included *M. avium* (n = 16) and *M. intracellulare* (n = 2).

Level of GPL Core IgA Antibody

The level of serum IgA antibody to GPL core was quantified using the EIA kit (Figure 1). As expected, patients with MAC-PD had significantly higher levels than patients with MAC contamination, those with pulmonary TB, those with other lung diseases, and healthy subjects—namely, 10.7 ± 7.9, 0.2 ± 0.1, 0.1 ± 0.1, 0.0 ± 0.1, and 0.0 ± 0.0 U/ml, respectively ($P < 0.0001$). A receiver operating characteristic (ROC) curve was constructed for MAC-PD and the other groups to establish the best cutoff value (Figure 2). Setting the cutoff value at 0.7 U/ml resulted in 100% specificity, at a sensitivity of 84.3% (Table E1). Using the EIA kit allowed clear discrimination between patients with MAC-PD and MAC contamination, pulmonary TB, and other lung diseases, as well as healthy subjects.

Next, we compared levels of serum IgA antibody to GPL core in fibrocavitary disease and NBE disease of MAC-PD. Significantly higher levels were found in NBE ($P < 0.05$) (Figure 3). With the cutoff value set at 0.7 U/ml, positivity in NBE and fibrocavitary disease was 91.4 and 63.2%, respectively. In contrast, in patients with MAC-PD, no significant differences between *M. avium* and *M. intracellulare* as causative agents were observed ($P = 0.403$). The erythrocyte sedimentation rate in MAC-PD was 32.6 ± 28.6 mm/hour and there was a significant positive correlation between the erythrocyte sedimentation rate and antibody levels in patients with MAC-PD ($r = 0.294$, $P < 0.05$).

Radiographic Severity and the Level of GPL Core Antibody

Forty-five patients with MAC-PD (10 with fibrocavitary disease, 26 with NBE disease, and 9 with unclassifiable type disease) underwent CCT and serodiagnosis at the same time. Four patients with unclassifiable type disease were excluded from the investigation because it was hard to discriminate between MAC lesions and underlying pulmonary disease. There was a positive correlation between the extent of disease and the

TABLE 1. CHARACTERISTICS OF STUDY SUBJECTS

	MAC-PD	MAC Contamination	Pulmonary TB	Other Lung Disease	Healthy Subjects
Number	70	18	36	45	76
Age, mean yr ± SD	68.0 ± 9.6	64.6 ± 11.6	52.9 ± 16.6*	66.3 ± 10.9	38.1 ± 12.0*
Age range, yr	50–90	28–78	24–76	29–82	20–65
Sex, no. male/no. female	25/45	10/8	26/10*	34/11*	41/35*
Duration of disease, mean yr ± SD	4.8 ± 4.6		0.3 ± 0.2	2.2 ± 2.4	

* $P < 0.001$.

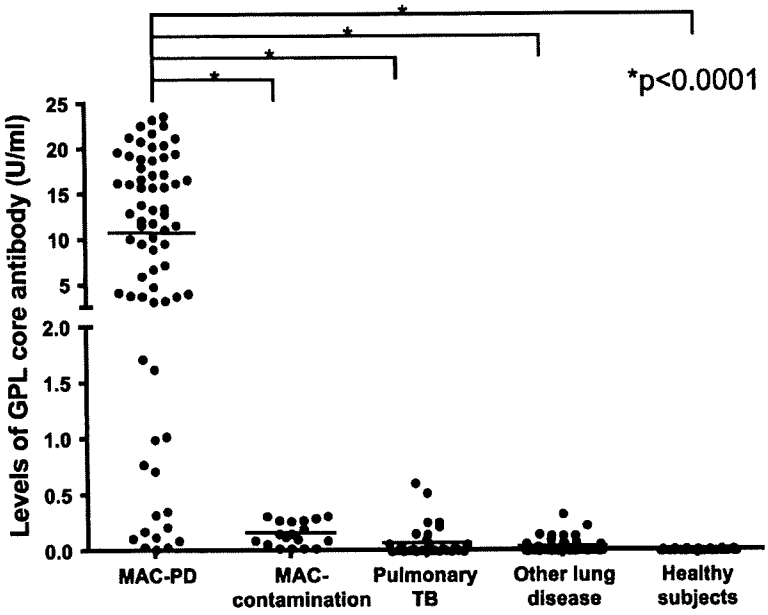

Figure 1. The level of serum IgA antibody to glycopeptidolipid (GPL) core antigen. Serum samples from six different institutions included 70 patients with *Mycobacterium avium* complex pulmonary disease (MAC-PD), 18 with MAC contamination, 37 with pulmonary tuberculosis (TB), 45 with other lung diseases, and 76 healthy subjects. Antibody levels in MAC-PD were significantly higher than in the other groups ($P < 0.0001$). All results are expressed as individual data, and *horizontal bars* indicate geometric means.

levels of the antibody ($r = 0.43$, $P < 0.05$) (Figure 4). The total numbers of involved segments were not different (7.8 ± 4.9 and 7.9 ± 4.2 in fibrocavitary and NBE disease, respectively). Of 26 patients with NBE disease, 9 had small thin wall cavities. A tendency toward elevated GPL core antibody levels was found in NBE patients with cavities compared with those without, but this trend was not statistically significant ($P = 0.08$).

DISCUSSION

We previously established a serologic test for MAC-PD using a mixture of GPLs and GPL core antigen, and reported the clinical application of the EIA method for quantifying antibody levels (7, 8). GPL is an antigen located on the surface of the MAC cell wall and determines the serotype. At present, 31 distinct serotype-specific GPLs have been identified, of which the complete structures of 14 have been identified (10–12). GPL consists of a core common to all MAC serotypes and a serotype-specific oligosaccharide. In the initial study to establish the serodiagnosis of MAC-PD, we used the whole GPL antigen, a mixture of 11 serotype-specific GPLs (7). We then found that the GPL core was the dominant antigenic epitope of GPL, and subsequently developed a serologic test using GPL core antigen (8). In the previous study, GPL core antibody (IgG, IgA, and IgM) levels were found to be elevated in sera of patients with MAC-PD, but not pulmonary TB, *M. kansasii*–PD, MAC colonization/contamination, and healthy subjects. The study showed that this serologic test was useful for diagnosing MAC-PD and for differentiating it from pulmonary TB and *M. kansasii*–PD. Consistent with this, Fujita and colleagues (13) reported elevated levels of antibody against the GPL core antigen in patients with MAC-PD but not in those with pulmonary TB. In our previous study (8), of the different Ig classes, best results were obtained by IgA, including an association with CCT findings. Thus, a higher level of serum IgA antibody to GPL core indicated a wider extent of MAC disease and larger nodule formation on CCT (9). Therefore, we have attempted to develop and to assess an EIA kit for quantifying serum IgA antibody to GPL core in the present study. Optical density levels were converted to U/ml using standard serum samples, which provided reliable and reproducible results. In this multicenter study, using the EIA kit, it was confirmed that patients with MAC-PD could be clearly differentiated from those with pulmonary TB, those with MAC contamination, those with other lung diseases, and healthy subjects. Similar to our previous studies (7–9), the sensitivity and specificity for diagnosing MAC-PD by the kit was high and the level of the antibody correlated with the extent of MAC-PD assessed using CCT.

Distinguishing pulmonary TB from MAC-PD in clinical practice using the EIA kit has proven useful. Differentiating TB from MAC is difficult because symptoms and radiographic findings are often similar among patients with pulmonary mycobacterial diseases. Patients with pulmonary TB require immediate treatment and isolation, whereas the diagnosis of MAC-PD does not necessitate rapidly starting antimicrobial therapy (1), and isolation is not required. GPL antigens, which are major cell surface antigens of MAC, are not present in the cell wall of *M. tuberculosis* complex (11). On the basis of this observation, patients with TB do not produce anti-GPL antibody. Indeed most patients with TB did not possess serum antibodies against GPLs (Figure 1) (7, 8). However, we cannot exclude the possibility that disease in patients with TB was of too short duration (MAC-PD, 4.8 ± 4.6 yr, vs. TB, 0.3 ± 0.2 yr) to have allowed immune responses and shed mycobacterial antigen. In this present study, with a cutoff level of 0.7 U/ml, all patients with TB were classified as seronegative. The levels of GPL core antibody in patients with pulmonary TB were very low or absent

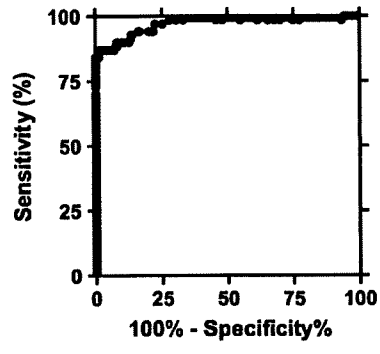

Figure 2. Receiver operating characteristic curve constructed for patients with *Mycobacterium avium*–complex pulmonary disease and the other groups.

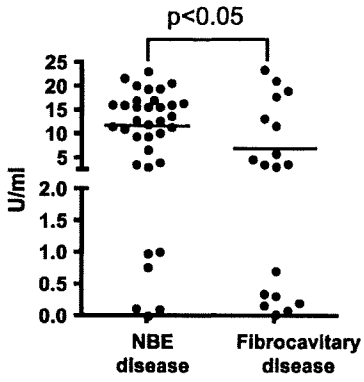

Figure 3. Levels of IgA antibody to glycopeptidolipid core antigens in nodular-bronchiectatic (NBE) and fibrocavitary subtypes of patients with *Mycobacterium avium* complex pulmonary disease (MAC-PD). Significantly higher levels were found in patients with MAC-PD with NBE compared with fibrocavitary disease ($P < 0.05$).

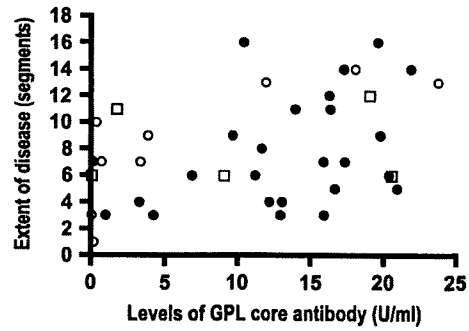

Figure 4. Correlation between antibody levels and radiographic severity using chest computed tomography in 41 patients with *Mycobacterium avium*–complex pulmonary disease. There was a positive correlation between the extent of disease and the levels of antibody ($r = 0.43$, $P < 0.05$). *Closed circles* represent patients with nodular-bronchiectatic disease, *open circles* represent patients with fibrocavitary disease, and *open squares* represent patients with unclassifiable type disease.

(0.1 ± 0.1 U/ml). In contrast, in previous studies (7, 8, 13), GPL seropositivity in patients with pulmonary TB ranged between 5.2 and 25%. One possible explanation for this previously reported lack of specificity may be that there was latent coinfection of MAC in patients with pulmonary TB. In the present study, however, we attempted to exclude patients with such latent coinfection because the entry criteria precluded patients having underlying lung disease or past history of pulmonary TB. Patients with lung diseases such as chronic obstructive pulmonary disease associated with smoking, bronchiectasis, previous mycobacterial disease, cystic fibrosis, and pneumoconiosis are prone to have MAC coinfection (1). In addition, future studies are needed to verify the cutoff value obtained from the ROC analysis using another sample of cases and controls on a much larger scale.

MAC-PD has recently been classified into two distinct subtypes: fibrocavitary disease and NBE disease (1). Fibrocavitary disease, the most common manifestation of MAC-PD, is usually seen in middle-aged or elderly men predisposed to lung disease due to smoking and alcohol drinking. This subtype of disease, generally progressive, is similar to pulmonary TB on chest radiography. If left untreated, it can lead to extensive lung destruction and death. In contrast, NBE disease is mostly seen in nonsmoking middle-aged or elderly women without predisposing lung disease. The clinical course is usually slower and less dramatic. Patients with NBE are presumed to have had a long subclinical period before appearance of disease manifestations. Significantly higher levels of GPL core antibody were seen in NBE than in fibrocavitary disease ($P < 0.05$) and higher seropositivity was found in patients with the former (91.4% compared with 63.2%). There were no significant differences of extent of disease between the two groups in patients who underwent CCT and serodiagnosis at the same time. Therefore, the results suggested the possibility that the antibody levels tend not to elevate in patients with fibrocavitary disease. This may reduce the utility of serodiagnosis for discriminating cavitary MAC from cavitary TB. However, the antibody would probably be present at high levels in patients with extensive lesions in fibrocavitary disease as was indeed found in three patients (17.9 ± 5.9 U/ml) who had extensive lesions (more than 13 segments) (Figure 4). Further investigations are required for confirmation of this notion in a larger study.

Of the 70 patients with MAC-PD, 64 had previously received combination chemotherapy, as recommended by the ATS guidelines (1). However, all had MAC-positive cultures at the time of serum collection, and were considered to have active MAC-PD. Thus, antibody levels were not changed by the failure of chemotherapy—that is, there was no conversion to seronegative from seropositive status (8); therefore, effects of the previous treatment on antibody levels were limited. Obviously, it would nonetheless be better to enroll chemotherapy-naive patients from diverse ethnic and racial populations and different geographic areas in future studies.

At present, the diagnosis of MAC-PD is usually made according to the ATS guidelines, which include clinical, radiographic, and microbiological criteria (1). The latter requires multiple positive cultures for MAC from sputum, a positive culture from bronchial lavage or a lung biopsy specimen, together with the other diagnostic features. Although it is easy to meet the criteria in advanced-stage MAC-PD, it is often difficult in early-stage disease. In clinical routine, it is impractical to obtain multiple sputum samples or perform bronchoscopy to obtain bronchial washings or lung tissue in all patients. It is also time consuming, because a long duration is required before the results of multiple cultures are available. There are several rapid methods for identification of MAC, but they have some limitations. The liquid culture–based system using radiometry and fluorometry allows the detection of mycobacterial growth at an early stage, fewer than 7 days for nontuberculous mycobacteria. However, limitations of this system include the inability to observe colony morphology, difficulty in recognizing mixed cultures, overgrowth by contaminations, cost, and radioisotope disposal. Rapid identification of MAC is also possible using DNA hybridization, nucleic acid amplification, or high-pressure liquid chromatography (1). The use of molecular biological technology has shortened the time required to identify mycobacteria from several weeks to as little as 1 day. The overall sensitivity for detecting MAC varies between 70 and 100%, with a specificity greater than 98%. However, the inability to distinguish live and dead organisms precludes nucleic acid amplification for definite diagnosis of active disease (14).

The EIA kit is a rapid (within a few hours) and noninvasive assay with high sensitivity (84.3%) and specificity (100%) for diagnosing MAC-PD. Using the EIA kit, as reported here, MAC-PD could be efficiently differentiated from MAC contamination. "MAC contamination" defined in the present study was considered to represent contamination from the environment, because patients were asymptomatic and revealed no significant CCT findings indicating active mycobacterial disease. Most of those people classified into the MAC contamination group were so categorized based on a single positive MAC culture by chance during the follow-up period after completion of chemotherapy for pulmonary TB or at routine examination on admission for other diseases. It is difficult to be certain that MAC contamina-

tion, as defined here, does not indicate subclinical infection because no confirmatory pathology was obtained. However, if MAC contamination does reflect subclinical infection, it is of little clinical importance and does not mandate therapy.

There were 15.7% false-negative EIA determinations in patients with MAC-PD. In such cases, diagnosis of MAC-PD should be made according to the ATS guidelines, as previously described. There are several possible explanations for these false-negative results, including the following: (*1*) recently diagnosed disease; (*2*) change of GPL core antigenicity after chemotherapy; or (*3*) diversity of immune responses to GPL core in individual patients, potentially governed by HLA genes (15). Therefore, it might be expected that not all patients with MAC-PD are capable of producing antibody to GPL core. Although the specificity determined here for the EIA kit was high, there remains also the possibility of false-positive results in patients with disease due to other mycobacteria, such as *Mycobacterium fortuitum*, *Mycobacterium chelonae*, *Mycobacterium abscessus*, and *Mycobacterium scrofulaceum*, because these organisms also possess GPL on their cell wall surface (10, 11, 16). Indeed, we have detected seropositivity in several patients with culture-positive *M. fortuitum* (data not shown). The incidence of pulmonary disease due to these other mycobacteria is relatively low (<5%) in Japan and the United States (6, 17), but a report from South Korea documented a high incidence of pulmonary infection by *M. abscessus* or *M. fortuitum* (33 and 11%, respectively (18). Therefore, caution is necessary when interpreting the results of the EIA kit in locations where other mycobacterial infections are endemic.

A recent study using high-resolution CT documented that characteristic findings with multiple small nodular shadows combined with bronchiectasis are predictive for culture-positive MAC with a relatively high probability. Swenson and colleagues (19) reported that, of 15 patients with these characteristic findings, 8 (53%) had cultures positive for MAC. Tanaka and coworkers (20) reported that, of 26 similar patients, 13 (50%) had positive cultures for MAC in bronchial washings. Therefore, combining positive results obtained by the EIA and the characteristic findings of high-resolution CT should yield a definitive diagnosis of MAC-PD even in patients with sputum culture–negative results for MAC. This approach may be useful especially in elderly patients with complications, in whom bronchoscopy cannot be performed.

In summary, the EIA kit for detection of serum IgA antibody specific for GPL core antigen is useful for rapid and accurate serodiagnosis of MAC-PD. Taken together with clinical, radiographic, and microbiological criteria, the kit may be a valuable tool for the diagnosis of MAC-PD. Validation of the EIA kit in the diagnosis of MAC-PD requires a larger controlled study in diverse populations.

Conflict of Interest Statement: None of the authors has a financial relationship with a commercial entity that has an interest in the subject of this manuscript.

References

1. Griffith DE, Aksamit T, Brown-Elliott BA, Catanzaro A, Daley C, Gordin F, Holland SM, Horsburgh R, Huitt G, Iademarco MF, *et al.*; ATS Mycobacterial Diseases Subcommittee. An official ATS/IDSA statement: diagnosis, treatment, and prevention of nontuberculous mycobacterial diseases. *Am J Respir Crit Care Med* 2007;175:367–416.
2. Subcommittee of the Joint Tuberculosis Committee of the British Thoracic Society. Management of opportunist mycobacterial infections: Joint Tuberculosis Committee guidelines 1999. *Thorax* 2000;55:210–218.
3. Field SK, Fisher D, Cowie RL. *Mycobacterium avium* complex pulmonary disease in patients without HIV infection. *Chest* 2004;126:566–581.
4. Field SK, Cowie RL. Lung disease due to the more common nontuberculous mycobacteria. *Chest* 2006;129:1653–1672.
5. Khan K, Wang J, Marras TK. Nontuberculous mycobacterial sensitization in the United States: national trends over three decades. *Am J Respir Crit Care Med* 2007;176:306–313.
6. Sakatani M. Nontuberculous mycobacteriosis: the present status of epidemiology and clinical studies. *Kekkaku* 1999;74:377–384.
7. Kitada S, Maekura R, Toyoshima N, Fujiwara N, Yano I, Ogura T, Ito M, Kobayashi K. Serodiagnosis of pulmonary disease due to *Mycobacterium avium* complex with an enzyme immunoassay that uses a mixture of glycopeptidolipid antigens. *Clin Infect Dis* 2002;35:1328–1335.
8. Kitada S, Maekura R, Toyoshima N, Naka T, Fujiwara N, Kobayashi M, Yano I, Ito M, Kobayashi K. Use of glycopeptidolipid core antigen for serodiagnosis of *Mycobacterium avium* complex pulmonary disease in immunocompetent patients. *Clin Diagn Lab Immunol* 2005;12:44–51.
9. Kitada S, Nishiuchi Y, Hiraga T, Naka N, Hashimoto H, Yoshimura K, Miki K, Miki M, Motone M, Fujikawa T, *et al.* Serological test and chest computed tomography findings in patients with *Mycobacterium avium* complex lung disease. *Eur Respir J* 2007;29:1217–1223.
10. Aspinall GO, Chatterjee D, Brennan PJ. The variable surface glycolipids of mycobacteria: structures, synthesis of epitopes, and biological properties. *Adv Carbohydr Chem Biochem* 1995;51:169–242.
11. Brennan PJ, Nikaido H. The envelope of mycobacteria. *Annu Rev Biochem* 1995;64:29–63.
12. Fujiwara N, Nakata N, Maeda S, Naka T, Doe M, Yano I, Kobayashi K. Structural characterization of a specific glycopeptidolipid containing a novel N-acyl-deoxy sugar from mycobacterium intracellulare serotype 7 and genetic analysis of its glycosylation pathway. *J Bacteriol* 2007;189:1099–1108.
13. Fujita Y, Doi T, Maekura R, Ito M, Yano I. Differences in serological responses to specific glycopeptidolipid-core and common lipid antigens in patients with pulmonary disease due to *Mycobacterium tuberculosis* and *Mycobacterium avium* complex. *J Med Microbiol* 2006;55:189–199.
14. Hellyer TJ, Fletcher TW, Bates JH, Stead WW, Templeton GL, Cave MD, Eisenach KD. Strand displacement amplification and the polymerase chain reaction for monitoring response to treatment in patients with pulmonary tuberculosis. *J Infect Dis* 1996;173:934–941.
15. Arend SM, Geluk A, van Meijgaarden KE, van Dissel JT, Theisen M, Andersen P, Ottenhoff TH. Antigenic equivalence of human T-cell responses to mycobacterium tuberculosis-specific RD1-encoded protein antigens ESAT-6 and culture filtrate protein 10 and to mixtures of synthetic peptides. *Infect Immun* 2000;68:3314–3321.
16. Chatterjee D, Khoo KH. The surface glycopeptidolipids of mycobacteria: structures and biological properties. *Cell Mol Life Sci* 2001;58:2018–2042.
17. O'Brien RJ, Geiter LJ, Snider DE Jr. The epidemiology of nontuberculous mycobacterial diseases in the United States: results from a national survey. *Am Rev Respir Dis* 1987;135:1007–1014.
18. Koh WJ, Kwon OJ, Jeon K, Kim TS, Lee KS, Park YK, Bai GH. Clinical significance of nontuberculous mycobacteria isolated from respiratory specimens in Korea. *Chest* 2006;129:341–348.
19. Swensen SJ, Hartman TE, Williams DE. Computed tomographic diagnosis of *Mycobacterium avium-intracellulare* complex in patients with bronchiectasis. *Chest* 1994;105:49–52.
20. Tanaka E, Amitani R, Niimi A, Suzuki K, Murayama T, Kuze F. Yield of computed tomography and bronchoscopy for the diagnosis of *Mycobacterium avium* complex pulmonary disease. *Am J Respir Crit Care Med* 1997;155:2041–2046.

JOURNAL OF BACTERIOLOGY, Feb. 2008, p. 1064–1071 Vol. 190, No. 3
0021-9193/08/$08.00+0 doi:10.1128/JB.01370-07

Identification and Characterization of Two Novel Methyltransferase Genes That Determine the Serotype 12-Specific Structure of Glycopeptidolipids of *Mycobacterium intracellulare*[▽]

Noboru Nakata,[1]* Nagatoshi Fujiwara,[2] Takashi Naka,[3] Ikuya Yano,[3] Kazuo Kobayashi,[4] and Shinji Maeda[5]

Department of Microbiology, Leprosy Research Center, National Institute of Infectious Diseases, Tokyo, Japan[1]; Department of Host Defense, Osaka City University Graduate School of Medicine, Osaka, Japan[2]; Japan BCG Laboratory, Tokyo, Japan[3]; Department of Immunology, National Institute of Infectious Diseases, Tokyo, Japan[4]; and Molecular Epidemiology Division, Mycobacterium Reference Center, The Research Institute of Tuberculosis, Japan Anti-Tuberculosis Association, Tokyo, Japan[5]

Received 23 August 2007/Accepted 5 November 2007

The *Mycobacterium avium* complex is distributed ubiquitously in the environment. It is an important cause of pulmonary and extrapulmonary diseases in humans and animals. The species in this complex produce polar glycopeptidolipids (GPLs); of particular interest is their serotype-specific antigenicity. Several reports have described that GPL structure may play an important role in bacterial physiology and pathogenesis and in the host immune response. Recently, we determined the complete structure of the GPL derived from *Mycobacterium intracellulare* serotype 7 and characterized the serotype 7 GPL-specific gene cluster. The structure of serotype 7 GPL closely resembles that of serotype 12 GPL, except for O methylation. In the present study, we isolated and characterized the serotype 12-specific gene cluster involved in glycosylation of the GPL. Ten open reading frames (ORFs) and one pseudogene were observed in the cluster. The genetic organization of the serotype 12-specific gene cluster resembles that of the serotype 7-specific gene cluster, but two novel ORFs (*orfA* and *orfB*) encoding putative methyltransferases are present in the cluster. Functional analyses revealed that *orfA* and *orfB* encode methyltransferases that synthesize *O*-methyl groups at the C-4 position in the rhamnose residue next to the terminal hexose and at the C-3 position in the terminal hexose, respectively. Our results show that these two methyltransferase genes determine the structural difference of serotype 12-specific GPL from serotype 7-specific GPL.

The *Mycobacterium avium* complex (MAC) consists of two species, *M. avium* and *Mycobacterium intracellulare*, which are opportunistic pathogens of humans and animals. Human exposure to the MAC is common because organisms of this complex are ubiquitous in the environment: they have been isolated from water, soil, plants, house dust, and other sources. In fact, the MAC is the most common cause of disease attributable to nontuberculous mycobacteria in humans (9). The majority of MAC infections are acquired environmentally, and person-to-person transmission is considered to be rare. The treatment of MAC infection is difficult because the organisms are often resistant to standard antituberculosis drugs.

Many antigenic or immunoregulatory glycolipids with structural diversity are expressed on the mycobacterial cell wall. These molecules are considered to be involved in bacterial virulence through host immune responses (5, 14, 22, 23). It is necessary to elucidate the molecular structure, biochemical characteristics, and biological functions of the lipid components to better understand the mechanisms of pathogenesis and drug resistance of the MAC. The most prominent feature of the MAC is the presence of antigenic glycolipids, the glycopeptidolipids (GPLs), which are present on the cell surface (1). The standard method for differentiation of MAC strains is serologic typing based on the oligosaccharide (OSE) residue of the GPL. GPLs contain a tetrapeptide-amino alcohol core, D-phenylalanine-D-*allo*-threonine-D-alanine-L-alaninol (D-Phe-D-*allo*-Thr-D-Ala-L-alaninol), with an amido-linked 3-hydroxy or 3-methoxy C_{26}-to-C_{34} fatty acid at the N terminus of D-Phe (4). The D-*allo*-Thr and terminal L-alaninol are further linked with 6-deoxy-talose (6-d-Tal) and 3,4-di-*O*-methyl-rhamnose (3,4-di-*O*-Me-Rha), respectively. This core GPL is present in all species of the MAC and shows a common antigenicity (1). In the serotype-specific GPLs, a haptenic OSE is linked with the 6-d-Tal residue. To date, 31 distinct serotype-specific polar GPLs have been identified biochemically; the complete structures of GPLs are partly defined for serotype 1 to 4, 7, 8, 9, 12, 14, 17, 19 to 21, 25, and 26 GPLs (7, 10). On the other hand, it has been reported that serotype-specific GPLs participate in pathogenesis and immunomodulation in the host (2, 13). Modification of the GPL structure might play an important role not only in antigenicity but also in host immune responses and bacterial physiology (18). Recently, chemical synthesis of various haptenic OSEs was demonstrated, and the genes encoding glycosylation pathway enzymes for the biosynthesis of GPLs were identified and characterized (8, 12, 19, 21). However, genes responsible for serotype-specific glycosylation have yet to be analyzed for most of the serotypes.

* Corresponding author. Mailing address: Department of Microbiology, Leprosy Research Center, National Institute of Infectious Diseases, 4-2-1 Aoba-cho, Higashimurayama, Tokyo 189-0002, Japan. Phone: 81 (42) 391 8211. Fax: 81 (42) 394 9092. E-mail: n-nakata@nih.go.jp.

▽ Published ahead of print on 16 November 2007.

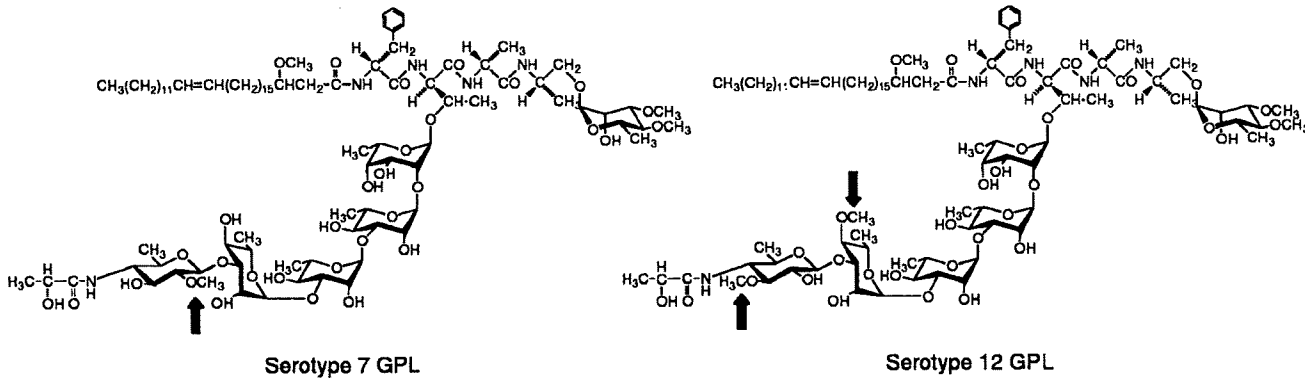

FIG. 1. Structures of serotype 7 and 12 GPLs. *O*-methyl groups specific to the serotypes are indicated by arrows.

In a previous study, we determined the complete structure of the GPL derived from *M. intracellulare* serotype 7 and characterized the serotype 7-specific gene cluster for GPL synthesis (10). The structure of serotype 7 GPL closely resembles that of serotype 12 GPL, except for O methylation (Fig. 1). In the present study, we determined the nucleotide sequence of the serotype 12-specific gene cluster involved in the glycosylation of the GPL and characterized two novel open reading frames (ORFs) encoding *O*-methyltransferases that determine the difference of serotype 12 GPL from serotype 7 GPL.

MATERIALS AND METHODS

Bacterial strains and construction of *M. intracellulare* cosmid library. *M. intracellulare* serotype 12 strain ATCC 35762 (NF 103), *M. intracellulare* serotype 7 strain ATCC 35847 (NF 027), and *M. intracellulare* serotype 7 strain NF 112 were used for this study. A cosmid library of *M. intracellulare* NF 103 was constructed as described previously (10). Briefly, genomic DNA of *M. intracellulare* NF 103 was prepared by mechanical disruption of bacterial cells in phosphate-buffered saline containing 50 mM EDTA, followed by phenol-chloroform extraction and precipitation with ethanol. Genomic DNA fragments randomly sheared to 30-kb to 50-kb fragments during the extraction process were fractionated and electroeluted from agarose gels. These DNA fragments were ligated to dephosphorylated arms of pYUB412 (XbaI-EcoRV and EcoRV-XbaI). After in vitro packaging using Gigapack III Gold extracts (Stratagene, La Jolla, CA), recombinant cosmids were introduced into *Escherichia coli* STBL2.

Isolation of cosmid clones carrying the GPL biosynthesis gene cluster and sequence analysis. PCR was used to isolate cosmid clones carrying the rhamnosyltransferase gene (*rtfA*), using primers rtfA-F (5′-TTTTGGAGCGACGAGTTCAT C-3′) and rtfA-R (5′-GTGTAGTTGACCACGCCGAC-3′). The insert of cosmid clone 161 was sequenced using a kit (BigDye Terminator cycle sequencing kit, version 3.1; Applied Biosystems, Foster City, CA) and a sequence analyzer (ABI Prism 310; Applied Biosystems). The putative function of each ORF was identified by similarity searches between the deduced amino acid sequences and those of known proteins, using BLAST (http://www.ncbi.nlm.nih.gov/BLAST/) and FramePlot (http://www.nih.go.jp/~jun/cgi-bin/frameplot.pl) with the DNASIS computer program (Hitachi Software Engineering, Yokohama, Japan).

Transformation of *M. intracellulare*. PCR was used to amplify and clone *orfA* and *orfB* into the plasmid vector pVV16. *M. intracellulare* NF 027 and NF 112 were transformed with the resultant plasmids by electroporation. Primers used to amplify *orfA*, *orfB*, and *orfA-orfB* were orfA-F (5′-GCGGATCCAGTGTGCAG ACGAGCGGAACT-3′), orfA-R (5′-GCGAATTCTTATCGAGAAAAAATA AAAG-3′), orfB-F (5′-GCGGATCCACTGCTAGACTCCGCCACCAT-3′), and orfB-R (5′-GCGAATTCCTACACCTTCACGGCGAGTC-3′).

Preparation of GPLs and OSE moieties. GPL 7 and GPL 12 were purified from *M. intracellulare* NF 027 and NF 103, respectively. The preparation of GPLs was performed as described previously (10, 15, 17). Briefly, each strain was grown in Middlebrook 7H9 broth (Difco Laboratories, Detroit, MI) with 0.5% glycerol and 10% Middlebrook oleic acid-albumin-dextrose-catalase enrichment (Difco Laboratories) at 37°C for 2 to 3 weeks. The heat-killed bacteria were sonicated and extracted using chloroform-methanol (2:1 [vol/vol]). The extractable lipids were hydrolyzed with 0.2 N sodium hydroxide in methanol at 37°C for 2 h. After neutralization using 6 N hydrochloride, chloroform-methanol (2:1 [vol/vol]) and water were added. The organic phase containing alkaline-stable lipids was recovered and evaporated, with subsequent addition of acetone to remove any acetone-insoluble components. The supernatant was dried up. It was then treated using a Sep-Pak silica cartridge (Waters Corp., Milford, MA) with washing (chloroform-methanol [95:5 {vol/vol}]) and elution (chloroform-methanol [1:1 {vol/vol}]) for partial purification. The GPL was then purified completely by preparative thin-layer chromatography (TLC) with silica gel G (Uniplate; 20 cm × 20 cm × 250 μm; Analtech, Inc., Newark, DE). The TLC was developed repeatedly, using chloroform-methanol-water (60:16:2 [vol/vol/vol]), until a single spot was obtained. To prepare the OSE moiety, purified GPL was processed using β-elimination with alkaline borohydride, and then the carbohydrate chain moiety

TABLE 1. Similarity of Orfs in *M. intracellulare* serotype 12 strain ATCC 35762 to known protein sequences

Orf	Predicted molecular mass (Da)	Predicted pI	Similar protein	Identity (no. of matched amino acids/total no. of amino acids)	E value	GenBank accession no.
GtfB	45,830	6.87	Glycosyltransferase GtfB	412/418	0.0	BAF45360
Orf1	45,203	6.10	Putative glycosyltransferase	414/417	0.0	BAF45361
OrfA	28,904	7.42	Putative methyltransferase	182/224	5e−88	NP_218045
OrfB	29,930	5.15	Putative methyltransferase	102/204	1e−19	EAZ88812
Orf3	32,151	10.41	Putative glycosyltransferase	196/223	1e−108	BAF45363
Orf4	40,742	5.41	Putative aminotransferase	338/374	0.0	BAF45364
Orf5	35,812	5.26	Hypothetical protein	303/329	4e−162	BAF45365
Orf7	27,693	5.99	Putative metallophosphoesterase	223/241	1e−122	BAF45367
Tn	28,538	11.85	Putative transposase	213/255	6e−107	AAL61662
Orf8	80,044	9.16	Putative acyltransferase	689/747	0.0	BAF45368
Orf9	37,797	8.26	Putative glycosyltransferase	310/337	7e−169	BAF45369
DrrC	28,549	12.01	Daunorubicin resistance protein C	261/263	3e−141	BAF45370

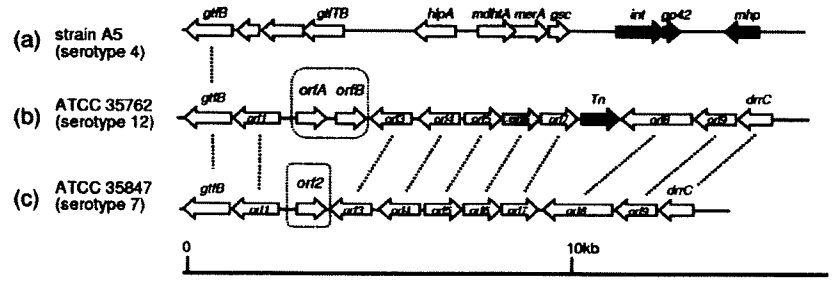

FIG. 2. Comparison of genetic organization of GPL biosynthesis clusters. (a) *M. avium* strain A5 organization, based on the annotated sequence obtained from GenBank (accession no. AY130970). (b) *M. intracellulare* ATCC 35762 (NF 103), sequenced in this study. (c) *M. intracellulare* ATCC 35847 (NF 027), sequenced in our previous study (GenBank accession no. AB274811). The orientation of each gene is shown by the arrow direction. The black arrows represent mobile elements, and the gray arrow represents a pseudogene. Mutually homologous ORFs and sequences are indicated with dotted lines.

elongated from D-*allo*-Thr was released as described previously (10, 15). Briefly, GPL was treated with 5 mg/ml sodium borohydride or borodeuteride in 0.5 N sodium hydroxide-ethanol (1:1 [vol/vol]) at 60°C for 16 h, with stirring. The reaction mixture was decationized with Dowex 50W X8 beads (The Dow Chemical Company, Midland, MI). The supernatant was collected and evaporated under nitrogen to remove boric acid. The dried residue was partitioned into two layers, using chloroform-methanol (2:1 [vol/vol]) and water. The upper aqueous phase was recovered and evaporated. In these processes, the OSE was purified as an oligoglycosyl alditol.

MALDI-TOF MS and MALDI-TOF/TOF MS analyses. The molecular species of the intact GPLs were detected using matrix-assisted laser desorption ionization–time-of-flight mass spectrometry (MALDI-TOF MS) with an Ultraflex II spectrophotometer (Bruker Daltonics, Billerica, MA). Each GPL was dissolved in chloroform-methanol (2:1 [vol/vol]) at a concentration of 1 mg/ml; 1 μl of a sample was then applied directly to the sample plate, followed by the addition of 1 μl of 10-mg/ml 2,5-dihydroxybenzoic acid in chloroform-methanol (1:1 [vol/vol]) as a matrix. The intact GPL was analyzed in the reflectron mode, with an accelerating voltage operating in positive mode at 20 kV (3). The OSE was analyzed by the fragment pattern with MALDI-TOF/TOF MS to determine the glycosyl composition. The OSE was dissolved with ethanol-water (3:7 [vol/vol]); the matrix was 10 mg/ml 2,5-dihydroxybenzoic acid in ethanol-water (3:7 [vol/vol]). The OSE and matrix were added to the sample plate by the same method as that for intact GPL. They were then analyzed in the lift-lift mode.

GC-MS analyses of alditol acetate derivatives. Gas chromatography (GC) and GC-MS analyses of partially methylated alditol acetate derivatives were performed to determine glycosyl compositions and linkage positions. Perdeuteromethylation was conducted using a modified procedure of Hakomori, as described previously (10, 11). Briefly, the dried OSE was dissolved with a mixture of dimethyl sulfoxide and sodium hydroxide, and deuteromethyl iodide was added. The reaction mixture was stirred at room temperature for 15 min, followed by the addition of water and chloroform. After centrifugation at 2,400 × *g* for 15 min, the upper water layer was discarded. The chloroform layer was washed twice with water and evaporated completely. To prepare partially deuteromethylated alditol acetates, perdeuteromethylated OSE was hydrolyzed using 2 N trifluoroacetic acid at 120°C for 2 h, reduced with 10 mg/ml sodium borodeuteride at 25°C for 2 h, and acetylated with acetic anhydride at 100°C for 1 h (6, 10, 16). GC-MS was then performed using a benchtop ion-trap mass spectrometer (Trace DSQ GC/MS; Thermo Electron Corporation, Austin, TX) equipped with a fused capillary column (30 m; 0.25-mm internal diameter) (Equity-1 or SP-2380; Supelco, Bellefonte, PA). Helium was used as the carrier gas, and the flow rate was 1 ml/min. The SP-2380 column was used for the analysis of alditol acetate derivatives. The temperature program was started at 60°C, with an increase of 40°C/min to 260°C and a hold at 260°C for 25 min. The Equity-1 column was used for analysis of perdeuteromethylated alditol acetate derivatives. The temperature program was 80°C for 1 min, with an increase of 20°C/min to 180°C followed by an increase of 8°C/min to 280°C.

Nucleotide sequence accession number. The nucleotide sequence reported here has been deposited in the NCBI GenBank database under accession number AB353739.

RESULTS

Cloning and sequence of the serotype 12 GPL biosynthesis cluster. To isolate the serotype 12-specific GPL biosynthesis gene cluster, a genomic cosmid library of an *M. intracellulare* serotype 12 strain, NF 103, was constructed. DNA was extracted from each clone by boiling. Using colony PCR with *rftA* primers, the positive clone 161 was isolated from the *E. coli* transductants. Sequencing analysis revealed that cosmid clone 161 carried the DNA region from *gtfB* to *drrC*. Ten ORFs and one pseudogene other than *gtfB* and *drrC* were observed in the cluster (Table 1 and Fig. 2). The genetic organization between the *gtfB* and *drrC* genes (15.6 kb) of *M. intracellulare* NF 103 (serotype 12) closely resembled that of

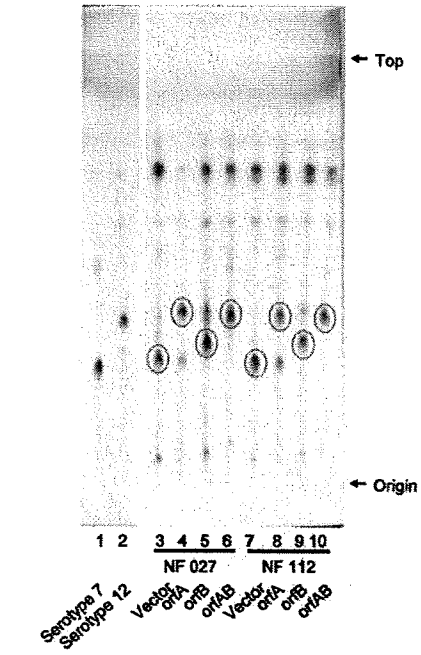

FIG. 3. TLC patterns of alkaline-stable lipids derived from *M. intracellulare* serotype 7 transformants. GPL 7 and GPL 12 were purified from *M. intracellulare* serotype 7 strain ATCC 35847 (NF 027) and serotype 12 strain ATCC 35762 (NF103). TLC was developed with a solvent system of chloroform-methanol-water (65:25:4 [vol/vol/vol]). Circled spots indicate prominent GPLs.

the same region of *M. intracellulare* NF 027 (serotype 7), except for three loci (Fig. 2). The first difference between them was an additional ORF encoding a transposase between *orf7* and *orf8* in NF 103 (Fig. 2). The second difference was that the *orf6* homologous sequence in NF 103 had a frame shift, indicating that this locus does not encode a protein. The third difference is that two novel ORFs (*orfA* and *orfB*) instead of *orf2* were found between *orf1* and *orf3* in NF 103.

Functional analysis of the two unique ORFs found in the serotype 12 GPL biosynthesis cluster. Based on sequence homology, *orfA* and *orfB* were able to encode methyltransferases responsible for producing serotype 12 GPLs (Table 1). We constructed three plasmids carrying *orfA* and/or *orfB* downstream of the *hsp-60* promoter to test this. These plasmids and a control vector plasmid were introduced individually into *M. intracellulare* serotype 7 (NF 027 and NF 112), and transformants were obtained. The GPLs produced from each transformant were analyzed.

The alkaline-stable lipids derived from six transformants of NF 027 and NF 112 in addition to the control strains (vector only) were developed by TLC, and the produced GPLs were compared to the spots of GPL 7 and GPL 12 (Fig. 3). The R_f values for GPLs synthesized in NF 027 transformed with *orfA* and NF 027 transformed with *orfA* and *orfB* (GPL 7-orfA and GPL 7-orfAB, respectively) were almost identical to that for GPL 12; the R_f value for the GPL synthesized in NF 027 transformed with *orfB* (GPL 7-orfB) was intermediate between those of GPL 7 and GPL 12, although the GPL synthesized in the control strain (GPL vector) was not changed from GPL 7. These results suggest that *orfA*, *orfB*, and *orfA-orfB* introduced into serotype 7 strain NF 027 were expressed and that they functioned for the modification of GPLs. We investigated the structural definition of these modified GPLs.

The GPLs produced in the transformants were purified using preparative TLC; their molecular weights were measured using MALDI-TOF MS (Fig. 4). The main molecularly related ions of GPL 7 and GPL 12 were detected as *m/z* 1,897 and 1,911, respectively, for $[M + Na]^+$ (Fig. 4a and b). The predominant *m/z* values were 1,911 for GPL 7-orfA, 1,897 for GPL 7-orfB, and 1,911 for GPL7-orfAB (Fig. 4c to e). The molecular weight of GPL 7-orfB was the same as that of GPL 7, and those of GPL 7-orfA and GPL 7-orfAB were equal to that of GPL 12. Next, MALDI-TOF/TOF MS analysis was performed to determine the glycosyl pattern, using fragment ions of glycosyl cleavage. The fragment ions of the GPL vector (equal to GPL 7) showed *m/z* 254, 400, 546, and 692 for cleavage in turn from terminal 4*N*-acyl-hexose (Hex) and 336, 482, and 628 for cleavage in the opposite direction from 6-d-Tal (Fig. 5a). The fragment ions of GPL 7-orfA, *m/z* 414 and 642, were different from those of GPL 7, i.e., *m/z* 400 and 628, respectively; they demonstrated that the mass number of the sugar next to the terminal Hex increased 14 mass units (Fig. 5b). This result suggests that the second sugar from the terminal one was changed from Rha to *O*-methyl rhamnose (*O*-Me-Rha). Similarly, the fragment pattern of GPL 7-orfAB was identical to that of GPL 7-orfA, although that of GPL 7-orfB was the same as that of GPL 7 (Fig. 5c and d). Altogether, GPL 7-orfAB was predicted to have a modification of the *O*-Me position in the terminal Hex along with the substitution of *O*-Me-Rha for Rha in the sugar next to the terminal Hex; GPL 7-orfB was modified only at the *O*-Me position in the terminal Hex.

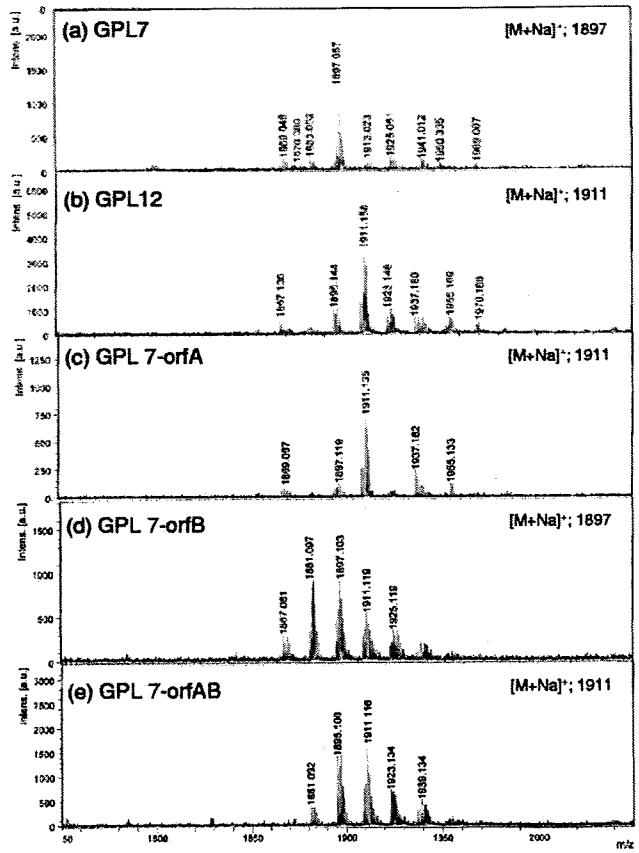

FIG. 4. MALDI-TOF MS spectra of GPLs derived from *M. intracellulare* serotype 7, serotype 12, and serotype 7 transformants. a.u., absorbance units.

GC-MS analyses of alditol acetate and perdeuteromethyl alditol acetate derivatives were performed to assign the linkage position of *O*-Me. As portrayed in Fig. 6a and b, the alditol acetate derivatives of the second sugar from the terminal 4*N*-acyl-Hex in GPL 7-orfA and GPL 7-orfB were assigned to 1,2,3,5-tetra-acetyl-4-*O*-methyl-rhaminitol (*m/z* 99, 131, 159, 201, and 261) and 1,2,3,4,5-penta-acetyl-rhaminitol (*m/z* 115, 157, 187, 217, 231, 289, and 303), respectively. The perdeuteromethyl alditol acetate derivatives of the terminal sugar in GPL 7-orfA and GPL 7-orfB were assigned to 3-*O*-deuteromethyl-1,5-di-*O*-acetyl-4-2′-*O*-deuteromethyl-propanoyl-deuteromethylamido-4,6-dideoxy-2-*O*-methyl-hexitol (*m/z* 105, 118, 165, 209, 222, 269, and 300) and 2-*O*-deuteromethyl-1,5-di-*O*-acetyl-4-2′-*O*-deuteromethyl-propanoyl-deuteromethylamido-4,6-dideoxy-3-*O*-methyl-hexitol (*m/z* 105, 121, 165, 206, 222, 266, and 300), respectively (Fig. 6c and d). In particular, the fragment ions of *m/z* 118 and 269 (Fig. 6c) versus *m/z* 121 and 266 (Fig. 6d) strongly indicated the different positions of linkages 2-*O*-Me and 3-*O*-Me. The alditol acetate and perdeuteromethyl alditol acetate derivatives in GPL 7-orfAB were detected with the same patterns of 4*N*-acyl-4,6-dideoxy-3-*O*-Me-Hex and 4-*O*-Me-Rha. According to these results, all OSE structures in GPLs derived from three serotype 7 transfor-

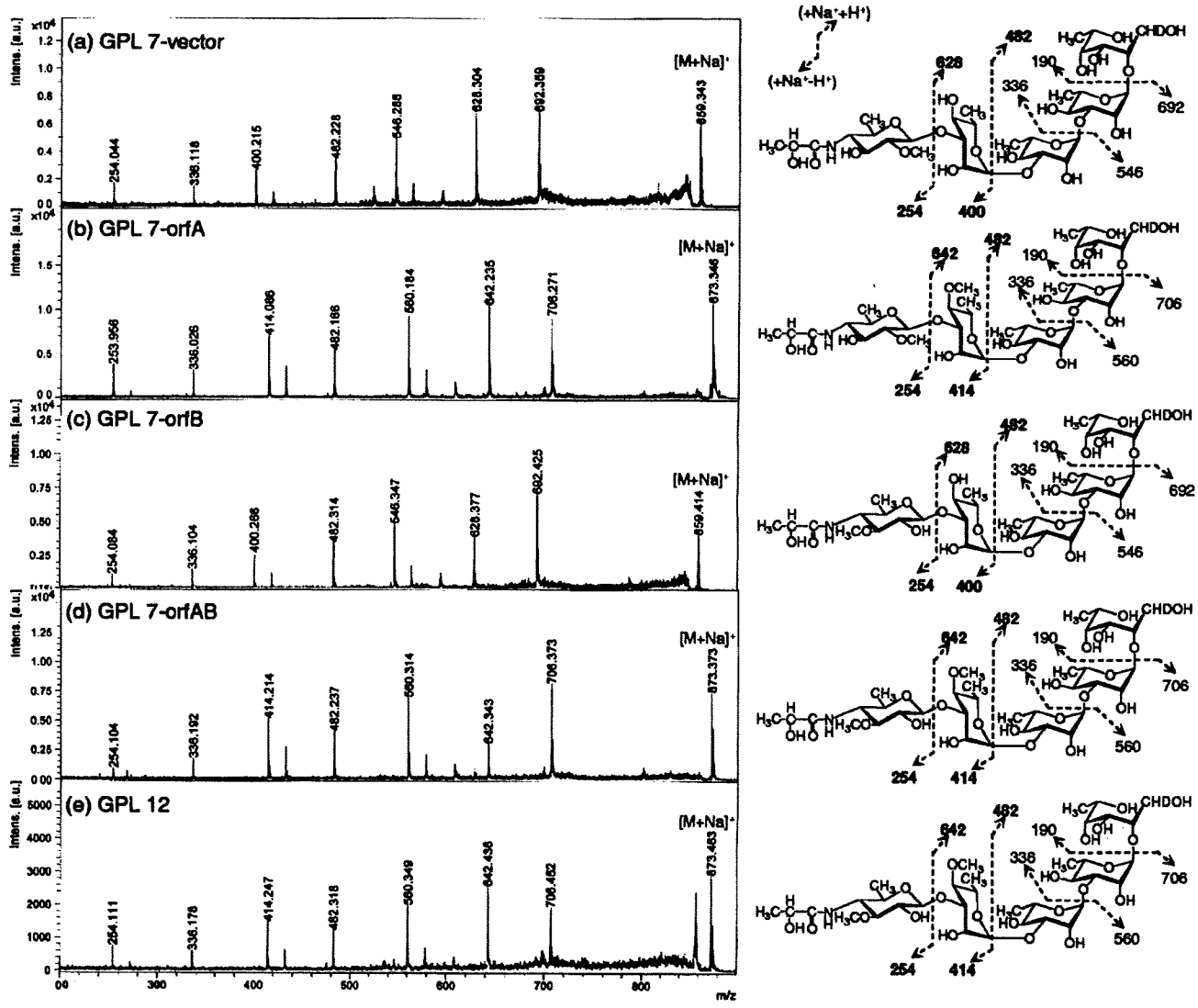

FIG. 5. Fragment patterns of MALDI-TOF/TOF MS spectra of OSEs in GPLs derived from *M. intracellulare* serotype 7, serotype 12, and serotype 7 transformants. The MALDI-TOF/TOF MS spectra were acquired using 10 mg/ml 2,5-dihydroxybenzoic acid in ethanol-water (3:7 [vol/vol]) as the matrix; the molecularly related ions were detected as $[M + Na]^+$ in lift-lift mode. The assigned fragment patterns of glycosyl residues are depicted. a.u., absorbance units.

mants were assigned as listed in Table 2. Altogether, the functions of the two genes were defined. The *orfA* product transfers a methyl group to the C-4 position of Rha next to the terminal sugar, and the *orfB* product transfers a methyl group to the C-3 position of the terminal sugar (Fig. 7). The results demonstrated that GPL 7 in the serotype 7 strain was changed completely to GPL 12 by introduction of the *orfA-orfB* gene cluster.

DISCUSSION

Nontuberculous mycobacteria, including the pathogenic species belonging to the MAC, have serotype-specific GPLs that are important components of the outer layer of the lipid-rich cell walls (5). Structural analyses of some serotype-specific GPLs derived from predominant clinical isolates have been reported (20). We recently determined the complete structure of serotype 7 GPL and the nucleotide sequence of the serotype 7-specific GPL biosynthesis cluster (10). In this cluster, Orfs 1, 3, and 9 might engender transfer of the two molecules of L-Rha and the terminal Hex of serotype 7 GPL (10). Orfs 4, 5, 7, and 8 are homologous to an aminotransferase, a carbamoyl phosphate synthase protein, a metallophosphoesterase, and an acyltransferase, respectively, and possibly relate to the biosynthesis of 2′-hydroxypropanoylamido in the terminal Hex. Based on analysis of sequence homology, these ORFs are probably responsible for the glycosylation of serotype 7 GPL. Serotype 12 GPL has a similar structure to that of serotype 7 GPL, except for O methylation (Fig. 1). In the present study, we cloned the serotype 12 GPL biosynthesis cluster and analyzed its sequence. Although the genetic organization of the *gtfB*-to-*drrC*

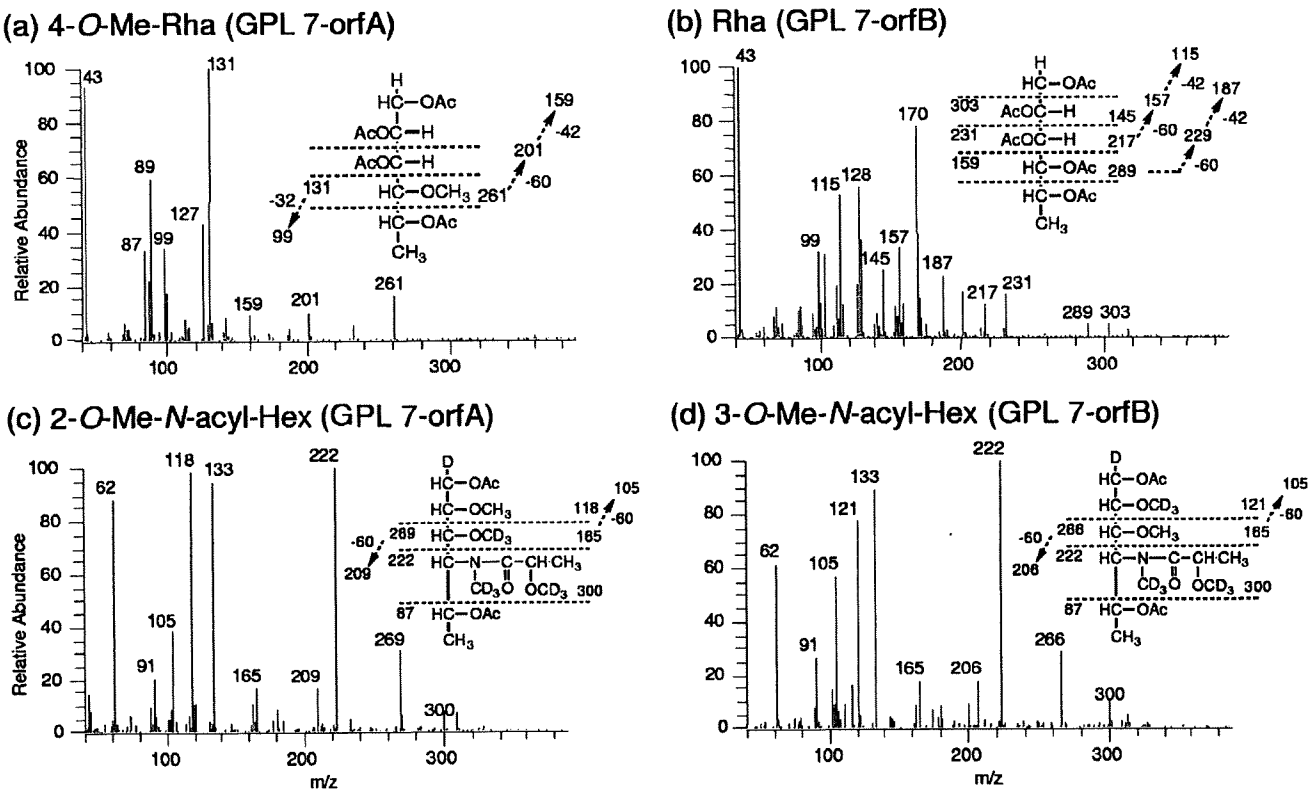

FIG. 6. Preparative GC-MS spectra of alditol acetate (a and b) and perdeuteromethylated alditol acetate (c and d) derivatives. The patterns of prominent fragment ions are presented. An SP-2380 column was used for the analysis of alditol acetate derivatives. The temperature program was started at 60°C, with an increase of 40°C/min to 260°C and a hold at 260°C for 25 min. An Equity-1 column was used for the perdeuteromethylated alditol acetate derivatives. The temperature program was 80°C for 1 min, with an increase of 20°C/min to 180°C followed by an increase of 8°C/min to 280°C.

region of the serotype 12 GPL biosynthetic cluster closely resembled that of serotype 7, significant differences were found in three loci (Fig. 2). The *M. intracellulare* serotype 12 strain NF 103 had one ORF encoding a transposase between *orf7* and *orf8* and had an *orf6* homologous sequence with frameshift inactivation. Orf6 in *M. intracellulare* serotype 7 exhibits sequence similarity to nucleotide sugar epimerases/dehydrogenases, but NF 112, one of the *M. intracellulare* serotype 7 isolates, had an interrupted *orf6* (10). These findings suggest that *orf6* is not involved in biosynthesis of either serotype 7 GPL or serotype 12 GPL. The most important difference between the two serotypes is that *M. intracellulare* serotype 12 had two unique ORFs, *orfA* and *orfB*, instead of *orf2* in *M. intracellulare* serotype 7. Actually, Orf2 in *M. intracellulare* serotype 7 was assigned to a methyltransferase and might be responsible for synthesis of the *O*-methyl group at the C-2 position in the terminal Hex. That possibility suggests that the two unique ORFs for serotype 12 encode *O*-methyltransferases that produce the serotype 12-specific structure. NF 027 (serotype 7) transformed with *orfA* produced 4*N*-acyl-4,6-dideoxy-2-*O*-Me-Hex→4-*O*-Me-Rha→Rha→Rha→6-d-Tal, indicating that the product from *orfA* had activity to synthesize an *O*-methyl group at C-4 in L-Rha next to the terminal Hex (Table 2 and Fig. 7). NF 027 transformed with *orfB* produced 4*N*-acyl-4,6-dideoxy-3-*O*-Me-Hex→Rha→Rha→Rha→6-d-Tal, indicating that the product from *orfB* had activity to synthesize an *O*-methyl group at C-3 in the terminal Hex. NF 027 transformed with *orfA* and *orfB* produced serotype 12-specific GPL,

TABLE 2. Summarized structures of OSEs derived from serotype 7 transformants

GPL	Molecular weight of OSE	Fragment ions in MALDI-TOF/TOF MS	*O*-Methyl group		Structure of OSE
			Terminal sugar	Residue next to terminal sugar	
GPL 7 vector	859	254, 400, 546, 692	2-*O*-Met		4*N*-acyl-4,6-dideoxy-2-*O*-Me-Hex→Rha→Rha→Rha→6-d-Tal
GPL 7-orfA	873	254, 414, 560, 706	2-*O*-Met	4-*O*-Met	4*N*-acyl-4,6-dideoxy-2-*O*-Me-Hex→4-*O*-Me-Rha→Rha→Rha→6-d-Tal
GPL 7-orfB	859	254, 400, 546, 692	3-*O*-Met		4*N*-acyl-4,6-dideoxy-3-*O*-Me-Hex→Rha→Rha→Rha→6-d-Tal
GPL 7-orfAB	873	254, 414, 560, 706	3-*O*-Met	4-*O*-Met	4*N*-acyl-4,6-dideoxy-3-*O*-Me-Hex→4-*O*-Me-Rha→Rha→Rha→6-d-Tal

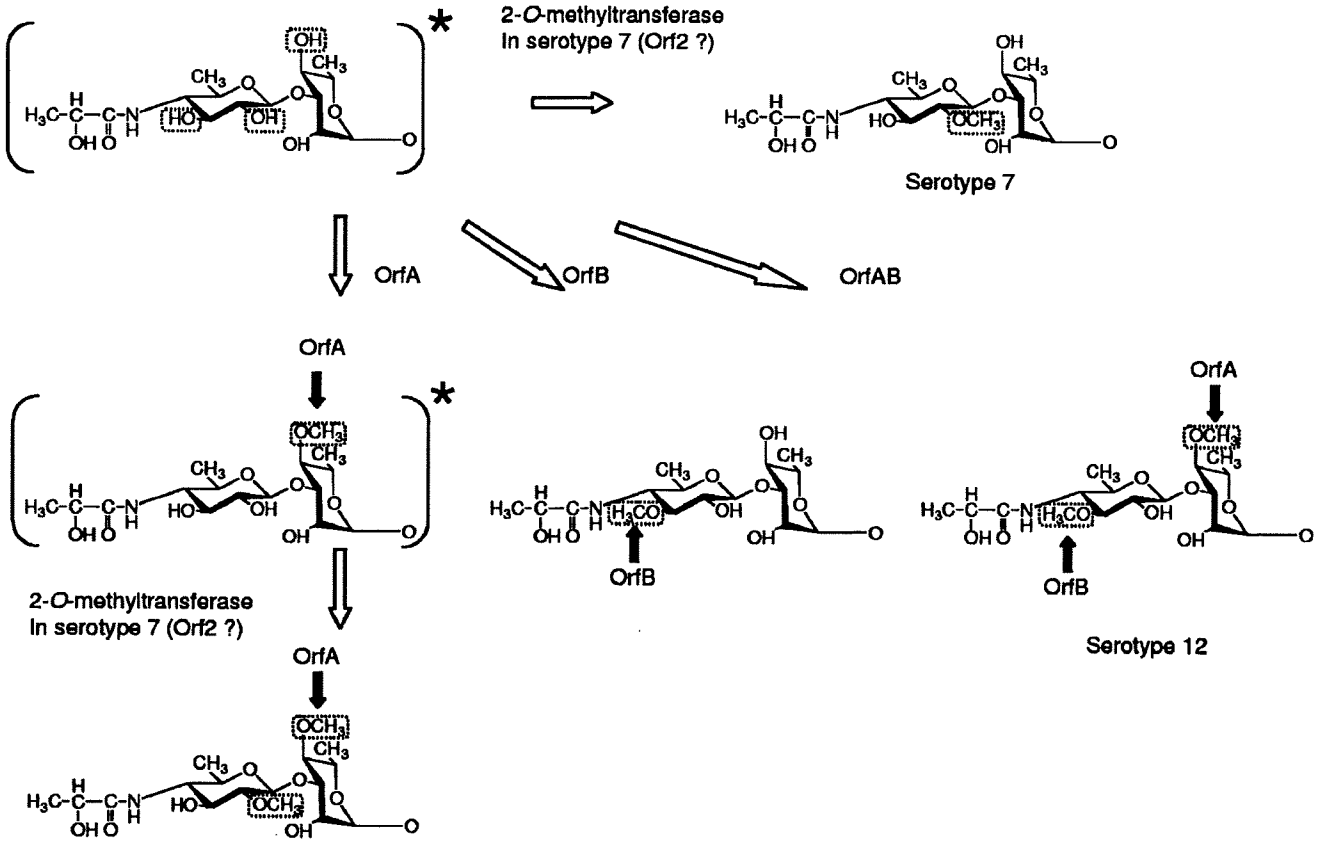

FIG. 7. Synthesis of *O*-methyl groups specific for GPL 7 and GPL 12 in the terminal disaccharide. The structures asterisked in the figure were not detected in this study. Serotype 12-specific O methylations and ORFs responsible for their syntheses are indicated by black arrows.

indicating that these two ORFs were responsible for producing the serotype 12-specific structure. The TLC patterns showed that the migration of GPL 7-orfB was different from that of GPL 7, although the MS data showed that they had the same molecular weight and the same number of methyl groups. A possible explanation for this is that a difference in the position of O methylation could influence hydrogen bond formation and the polarity of the whole molecule and consequently result in a different TLC migration pattern. GPL 7-orfB had an *O*-methyl group at C-3 but not at C-2 in the terminal Hex, indicating that the reaction of O methylation at C-2 by the 2-*O*-methyltransferase in serotype 7 is strongly inhibited by *O*-methylation at C-3. In addition, NF 027 transformed with *orfA* produced a trace of serotype 7-specifc GPL (Fig. 3, lane 4), and NF 027 transformed with *orfA* and *orfB* produced only serotype 12 GPL (Fig. 3, lane 6), suggesting that O methylation at C-2 in the terminal Hex might hinder the reaction of O methylation at C-4 in Rha next to the terminal Hex or that O methylation at C-3 in the terminal Hex might promote the reaction of O methylation at C-4 in Rha.

Because it is not likely that *M. intracellulare* serotypes 7 and 12 independently acquired different methyltransferase genes in the same genetic location between *orf1* and *orf3*, the common ancestor for these two serotypes possibly had all three genes and activated them as the occasion demanded. However, our results showed that reactions of O methylation at C-3 and C-2 in the terminal Hex were competitive (Fig. 3, lane 5, and Table 2). Tsang et al. (26) reported that the frequency of isolation of MAC organisms from AIDS or non-AIDS patients varied among serotypes and that *M. intracellulare* serotype 12 was isolated more often than serotype 7. These two serotypes of *M. intracellulare* might have evolved to adapt to certain environments by losing *orf2* or *orfA-orfB*.

Actually, GPLs are among the immunogenic molecules of the MAC. Tassel et al. reported that the core GPL seems to play a role in suppression of a mitogen-induced blastogenic response of spleen cells (25); furthermore, our previous study showed that sera of patients with MAC disease contain antibodies against GPLs and that the antibody level reflects disease activity (17). In addition, the immunomodulating activity of GPLs on macrophage functions is serotype dependent (13, 24). Elucidation of the structure-activity relationship of GPLs is necessary to better understand the pathogenesis of MAC infection.

ACKNOWLEDGMENTS

This work was supported by grants from the Ministry of Health, Labor and Welfare (Emerging and Re-Emerging Infectious Diseases), the Ministry of Education, Culture, Sports, Science and Technology of Japan, and the Japan Health Sciences Foundation.

N.N. is grateful to M. Kai and M. Makino for helpful discussions.

REFERENCES

1. **Aspinall, G. O., D. Chatterjee, and P. J. Brennan.** 1995. The variable surface glycolipids of mycobacteria: structures, synthesis of epitopes, and biological properties. Adv. Carbohydr. Chem. Biochem. **51**:169–242.
2. **Barrow, W. W., T. L. Davis, E. L. Wright, V. Labrousse, M. Bachelet, and N. Rastogi.** 1995. Immunomodulatory spectrum of lipids associated with *Mycobacterium avium* serovar 8. Infect. Immun. **63**:126–133.
3. **Bhatt, A., N. Fujiwara, K. Bhatt, S. S. Gurcha, L. Kremer, B. Chen, J. Chan, S. A. Porcelli, K. Kobayashi, G. S. Besra, and W. R. Jacobs.** 2007. Deletion of *kasB* in *Mycobacterium tuberculosis* causes loss of acid-fastness and subclinical latent tuberculosis in immunocompetent mice. Proc. Natl. Acad. Sci. USA **104**:5157–5162.
4. **Brennan, P. J., and M. B. Goren.** 1979. Structural studies on the type-specific antigens and lipids of the *Mycobacterium avium-Mycobacterium intracellulare-Mycobacterium scrofulaceum* serocomplex. *Mycobacterium intracellulare* serotype 9. J. Biol. Chem. **254**:4205–4211.
5. **Brennan, P. J., and H. Nikaido.** 1995. The envelope of mycobacteria. Annu. Rev. Biochem. **64**:29–63.
6. **Chatterjee, D., G. O. Aspinall, and P. J. Brennan.** 1987. The presence of novel glucuronic acid-containing, type-specific glycolipid antigens within *Mycobacterium spp*. Revision of earlier structures. J. Biol. Chem. **262**:3528–3533.
7. **Chatterjee, D., and K. H. Khoo.** 2001. The surface glycopeptidolipids of mycobacteria: structures and biological properties. Cell. Mol. Life Sci. **58**: 2018–2042.
8. **Eckstein, T. M., J. T. Belisle, and J. M. Inamine.** 2003. Proposed pathway for the biosynthesis of serovar-specific glycopeptidolipids in *Mycobacterium avium* serovar 2. Microbiology **149**:2797–2807.
9. **Falkinham, J. O.** 1996. Epidemiology of infection by nontuberculous mycobacteria. Clin. Microbiol. Rev. **9**:177–215.
10. **Fujiwara, N., N. Nakata, S. Maeda, T. Naka, M. Doe, I. Yano, and K. Kobayashi.** 2007. Structural characterization of a specific glycopeptidolipid containing a novel *N*-acyl-deoxy sugar from *Mycobacterium intracellulare* serotype 7 and genetic analysis of its glycosylation pathway. J. Bacteriol. **189**:1099–1108.
11. **Hakomori, S.** 1964. A rapid permethylation of glycolipid, and polysaccharide catalyzed by methylsulfinyl carbanion in dimethyl sulfoxide. J. Biochem. (Tokyo) **55**:205–208.
12. **Heidelberg, T., and O. R. Martin.** 2004. Synthesis of the glycopeptidolipid of *Mycobacterium avium* serovar 4: first example of a fully synthetic C-mycoside GPL. J. Org. Chem. **69**:2290–2301.
13. **Kano, H., T. Doi, Y. Fujita, H. Takimoto, I. Yano, and Y. Kumazawa.** 2005. Serotype-specific modulation of human monocyte functions by glycopeptidolipid (GPL) isolated from *Mycobacterium avium* complex. Biol. Pharm. Bull. **28**:335–339.
14. **Kaufmann, S. H.** 2001. How can immunology contribute to the control of tuberculosis? Nat. Rev. Immunol. **1**:20–30.
15. **Khoo, K. H., D. Chatterjee, A. Dell, H. R. Morris, P. J. Brennan, and P. Draper.** 1996. Novel O-methylated terminal glucuronic acid characterizes the polar glycopeptidolipids of *Mycobacterium habana* strain TMC 5135. J. Biol. Chem. **271**:12333–12342.
16. **Khoo, K. H., E. Jarboe, A. Barker, J. Torrelles, C. W. Kuo, and D. Chatterjee.** 1999. Altered expression profile of the surface glycopeptidolipids in drug-resistant clinical isolates of *Mycobacterium avium* complex. J. Biol. Chem. **274**:9778–9785.
17. **Kitada, S., R. Maekura, N. Toyoshima, N. Fujiwara, I. Yano, T. Ogura, M. Ito, and K. Kobayashi.** 2002. Serodiagnosis of pulmonary disease due to *Mycobacterium avium* complex with an enzyme immunoassay that uses a mixture of glycopeptidolipid antigens. Clin. Infect. Dis. **35**:1328–1335.
18. **Krzywinska, E., S. Bhatnagar, L. Sweet, D. Chatterjee, and J. S. Schorey.** 2005. *Mycobacterium avium* 104 deleted of the methyltransferase D gene by allelic replacement lacks serotype-specific glycopeptidolipids and shows attenuated virulence in mice. Mol. Microbiol. **56**:1262–1273.
19. **Maslow, J. N., V. R. Irani, S. H. Lee, T. M. Eckstein, J. M. Inamine, and J. T. Belisle.** 2003. Biosynthetic specificity of the rhamnosyltransferase gene of *Mycobacterium avium* serovar 2 as determined by allelic exchange mutagenesis. Microbiology **149**:3193–3202.
20. **McNeil, M., A. Y. Tsang, and P. J. Brennan.** 1987. Structure and antigenicity of the specific oligosaccharide hapten from the glycopeptidolipid antigen of *Mycobacterium avium* serotype 4, the dominant mycobacterium isolated from patients with acquired immune deficiency syndrome. J. Biol. Chem. **262**: 2630–2635.
21. **Miyamoto, Y., T. Mukai, N. Nakata, Y. Maeda, M. Kai, T. Naka, I. Yano, and M. Makino.** 2006. Identification and characterization of the genes involved in glycosylation pathways of mycobacterial glycopeptidolipid biosynthesis. J. Bacteriol. **188**:86–95.
22. **Porcelli, S. A., and R. L. Modlin.** 1999. The CD1 system: antigen-presenting molecules for T cell recognition of lipids and glycolipids. Annu. Rev. Immunol. **17**:297–329.
23. **Smith, I.** 2003. *Mycobacterium tuberculosis* pathogenesis and molecular determinants of virulence. Clin. Microbiol. Rev. **16**:463–496.
24. **Takegaki, Y.** 2000. Effect of serotype specific glycopeptidolipid (GPL) isolated from *Mycobacterium avium* complex (MAC) on phagocytosis and phagosome-lysosome fusion of human peripheral blood monocytes. Kekkaku **75**:9–18.
25. **Tassell, S. K., M. Pourshafie, E. L. Wright, M. G. Richmond, and W. W. Barrow.** 1992. Modified lymphocyte response to mitogens induced by the lipopeptide fragment derived from *Mycobacterium avium* serovar-specific glycopeptidolipids. Infect. Immun. **60**:706–711.
26. **Tsang, A. Y., J. C. Denner, P. J. Brennan, and J. K. McClatchy.** 1992. Clinical and epidemiological importance of typing of *Mycobacterium avium* complex isolates. J. Clin. Microbiol. **30**:479–484.

RESEARCH ARTICLE

$CD4^+$ T-cell activation by antigen-presenting cells infected with urease-deficient recombinant *Mycobacterium bovis* bacillus Calmette-Guérin

Tetsu Mukai, Yumi Maeda, Toshiki Tamura, Yuji Miyamoto & Masahiko Makino

Department of Microbiology, Leprosy Research Center, National Institute of Infectious Diseases, Tokyo, Japan

Correspondence: Masahiko Makino, Department of Microbiology, Leprosy Research Center, National Institute of Infectious Diseases, 4-2-1 Aobacho, Higashimurayama, Tokyo 189-0002, Japan. Tel.: +81 42 391 8059; fax: +81 42 391 8212; e-mail: mmaki@nih.go.jp

Received 22 November 2007; revised 11 February 2008; accepted 15 February 2008. First published online 9 April 2008.

DOI:10.1111/j.1574-695X.2008.00407.x

Editor: Patrick Brennan

Keywords
BCG; urease; macrophage; dendritic cell.

Abstract

We constructed a recombinant *Mycobacterium bovis* bacillus Calmette-Guérin (BCG-ΔUT) that lacks urease, providing acidic intraphagosomal conditions to drive an effective human immune T-cell response. BCG-ΔUT-infected macrophages stimulated autologous $CD4^+$ T cells more efficiently than parent BCG-infected macrophages. For further T-cell activation, BCG-ΔUT-infected macrophages required pretreatment with exogenous recombinant granulocyte-macrophage colony-stimulating factor or costimulation with either CD40 ligand or interferon-γ. By contrast, BCG-ΔUT-infected dendritic cells induced significant activation of naïve $CD4^+$ T cells without costimulating signals. C57BL/6 mice intradermally inoculated with BCG-ΔUT more efficiently produced memory T cells that responded to recall antigen. Therefore, the depletion of urease from BCG is useful for the activation of T cells.

Introduction

Mycobacteria, such as *Mycobacterium leprae* and *Mycobacterium tuberculosis*, are representative parasitic intracellular pathogens. *Mycobacterium leprae* is a causative agent of human leprosy, in cases of which skin lesions and chronic progressive peripheral nerve injury are usually observed (Stoner, 1979; Job, 1989). At present, around one-third of individuals are infected with *M. tuberculosis* and several millions die as result of tuberculosis each year (Dye *et al.*, 2005; World Health Organization, 2006). *Mycobacterium bovis* bacillus Calmette-Guérin (BCG) has been used as a vaccine against leprosy, although its efficacy is quite limited (Andersen & Doherty, 2005; Setia *et al.*, 2006). The emergence of multidrug-resistant strains of these mycobacteria is of concern (Maeda *et al.*, 2001; Kai *et al.*, 2004; Kaufmann, 2005), and therefore the urgent development of a new vaccine, including a more efficacious recombinant BCG, is desired (Kaufmann, 2005).

Among various immunocompetent cells, $CD4^+$ T cells, especially IFN-γ-producing cells, play an extremely important role in inhibiting the multiplication of mycobacteria, killing them in the early stages of infection, and keeping the bacterial load at a stable level (Orme *et al.*, 1993; Dockrell *et al.*, 1996; Hashimoto *et al.*, 2002). $CD4^+$ T cells that can respond quickly to pathogenic mycobacteria and produce IFN-γ are known as memory T cells. The efficient production of such memory T cells needs pre-exposure to antigenic vaccinating molecules, which share their antigenicity with that of pathogenic mycobacteria (Kaufmann, 2006). BCG has been considered a good candidate for a vaccine against *M. leprae* in this respect, however its efficacy is limited in several aspects, including the ability to activate T cells (Kaufmann & McMichael, 2005). BCG resides in the phagosomes of macrophages and thus attenuates the trafficking of antigenic molecules to the macrophage cell surface (Grode *et al.*, 2005). One possible strategy for improving the ability of BCG to stimulate T cells is to enhance its ability to fuse with the lysosomes. To this end, we knocked out the *urease* gene from BCG. The urease-deficient recombinant BCG (BCG-ΔUT) is expected to allow phagosomal acidification in the host cells, and induce efficient phagosome maturation for cytolytic activity of the antigenic molecules of BCG (Schaible *et al.*, 1998; Honerzu Bentrup & Russell, 2001).

In the present study, we evaluated the ability of BCG-ΔUT to activate IFN-γ-producing type 1 $CD4^+$ T cells through

antigen-presenting cells (APCs), and to produce memory $CD4^+$ T cells. When used as a target of BCG-ΔUT, macrophages fully stimulated $CD4^+$ T cells in the presence of costimulatory agents such as CD40 ligand (L) and IFN-γ. In addition, BCG-ΔUT-infected monocyte-derived dendritic cells (DCs) activated type 1 $CD4^+$ T cells more efficiently than parent BCG-infected cells in the absence of these costimulators. Therefore, BCG-ΔUT was found to be a useful T-cell-stimulating agent.

Materials and methods

Preparation of blood cells

Peripheral blood was obtained from healthy purified protein derivative (PPD)-positive individuals with informed consent. PPD-negative individuals provide more information, however, as healthy individuals are PPD-positive, due to compulsory BCG vaccination for children in Japan (0–4 years old). Peripheral blood mononuclear cells (PBMCs) were isolated using Ficoll-Paque Plus (Pharmacia, Uppsala, Sweden) and cryopreserved in liquid nitrogen until use, as previously described (Makino & Baba, 1997). For the preparation of peripheral monocytes, $CD3^+$ T cells were removed from either freshly isolated heparinized blood, or cryopreserved PBMCs using immunomagnetic beads coated with anti-CD3 monoclonal antibody (mAb) (Dynabeads 450, Dynal, Oslo, Norway). The $CD3^-$ PBMC fraction was plated on collagen-coated plates and nonadherent cells were removed by extensive washing. The remaining adherent cells were used as monocytes (Makino & Baba, 1997). Macrophages were generated by culturing monocytes in the presence of 20% fetal calf serum and recombinant (r) macrophage colony-stimulating factor (M-CSF) (R&D Systems, Abingdom, UK) (Makino *et al.*, 2007). Macrophages were pulsed with rBCGs on day 5 of culture, and were used as a stimulator of T cells on day 7 (Makino *et al.*, 2007). Monocyte-derived DCs were differentiated as described previously (Makino *et al.*, 1999). Briefly, monocytes were cultured in the presence of 50 ng recombinant granulocyte-macrophage colony-stimulating factor (GM-CSF; Pepro Tech EC Ltd, London, UK) and 10 ng of recombinant interleukin (rIL)-4 (Pepro Tech) per millilitre (Makino *et al.*, 1999). On day 3 of culture, immature DCs were infected with rBCGs at the indicated multiplicity of infection (MOI), and on day 5 of culture, DCs were used for further analyses of surface antigens and for mixed-lymphocyte assays.

BCG culture and DNA manipulation

The mycobacterial strain, BCG substrain Tokyo, for DNA manipulation was grown in Middlebrook 7H9 broth (Difco Laboratories) with 0.05% Tween 80 or Middlebrook 7H10 agar (Difco) with 0.5% glycerol, each supplemented with 10% albumin–dextrose–catalase enrichment (Difco). DNA manipulations including isolation of DNA, transformation and PCR, were carried out as described previously (Miyamoto *et al.*, 2004). *Escherichia coli* strain DH5α was used for routine manipulation and the propagation of plasmid DNA. *Escherichia coli* strain STBL4 was used for the construction of plasmid vectors derived from phAE87. Antibiotics were added as required: hygromycin B, 150 μg mL^{-1} for *E. coli* and 75 μg mL^{-1} for *Mycobacterium smegmatis* (mc^2155) and *M. bovis* BCG. A recombinant BCG that lacks a *urease* gene was constructed. The sequence of the targeted gene, *ureC* (BCG 1886), was obtained from the BCG list (http://genolist.pasteur.fr/BCGList/). The *ureC* gene was inactivated by inserting a hygromycin-resistance cassette (*hyg*) using a specialized transducing phage system for homologous recombination (Bardarov *et al.*, 2002; Miyamoto *et al.*, 2006). To construct the disrupted sequence, fragments of around 0.9 kb both upstream and downstream of *ureC* were amplified from BCG-Tokyo genomic DNA using the following two pairs of primers: F UureC and R UureC for upstream of *ureC*, and F DureC and R DureC for downstream of *ureC*. The PCR products were digested with each restriction enzyme and cloned into the corresponding site flanking *hyg* of pYUB854 to give pYUB854-ureC-UD. This plasmid was used for packaging into the phasmid vector phAE87 to construct a specialized transducing mycobacteriophage for gene disruption as described previously (Bardarov *et al.*, 2002; Miyamoto *et al.*, 2006). BCG-Tokyo infected with the mycobacteriophage at an MOI of 50 was incubated at 37 °C for 3 h in 7H9 broth without Tween 80. Harvested bacterial cells were then plated and cultured on 7H10 agar containing hygromycin B (75 μg mL^{-1}) for 3 weeks. The hygromycin B-resistant colonies were selected and evaluated with a conventional urease assay. A change in the color of the assay medium from yellowish to red was scored as urease-positive. Furthermore, genomic DNA obtained from these colonies was subjected to PCR to confirm the disruption of the gene using primers F ureC and R ureC (Fig. 1). The colony which tested negative in the urease assay was named BCG-ΔUT, while the parental BCG substrain Tokyo is referred to as BCG-Tokyo.

Preparation of *M. leprae*

Mycobacterium leprae (Thai-53) was isolated from the footpads of BALB/c-*nu/nu* mice (McDermott-Lancaster *et al.*, 1987). The isolated bacteria were counted by Shepard's method (Charles & Shepard, 1960). The MOI for infection to host cells was determined based on the assumption that macrophages and DCs were equally susceptible to infection with BCG or *M. leprae* (Hashimoto *et al.*, 2002).

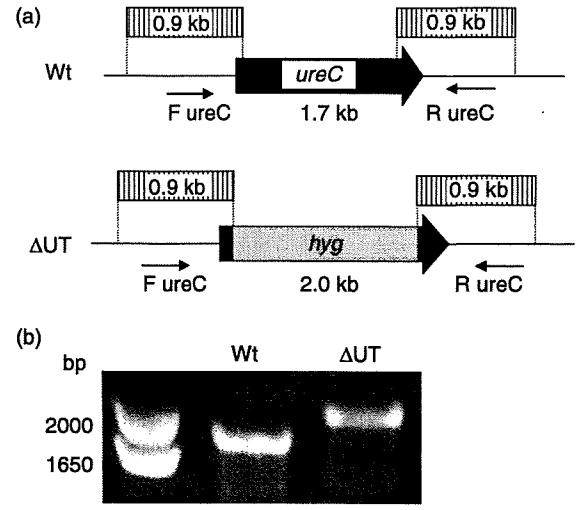

Fig. 1. Disruption of the *ureC* gene. (a) Schematic diagram of the *ureC* region on the chromosome of the wild-type *Mycobacterium bovis* BCG Tokyo strain and its gene disruptant, ΔUT. The shaded boxes indicate the regions included in the recombinant phage for gene disruption. The black arrow represents the coding region of the *ureC* gene. The gray box represents the hygromycin-resistace cassette (*hyg*). The primers used for PCR analysis are indicated by small arrows. (b) PCR analysis of the wild-type and the disruptant using the primers indicated above.

Preparation of mycobacterial antigen

The cytosolic fraction of BCG-Tokyo (BCC) was obtained as described previously (Maeda *et al.*, 2003). Briefly, the mycobacterial suspension containing the protease inhibitors was mixed with zirconium beads at a ratio of *c.* 1 : 1 (v/v) and homogenized using a Beads Homogenizer Model BC-20 (Central Scientific Commerce, Tokyo). The suspension was centrifuged at 10 000 *g* to remove the cell-wall fractions. The supernatant was then ultracentrifuged at 100 000 *g* and the resulting supernatant was taken as the cytosolic fraction. For preparation of the *M. leprae* membrane (MLM) fraction, *M. leprae* was used instead of BCG and treated similarly. The pellet obtained by ultracentrifugation (100 000 *g* for 1 h) was used as a membrane fraction (MLM). The optimal concentration of BCC and MLM for stimulating T cells was determined in advance.

Analysis of cell surface antigens

The expression of cell surface antigens on macrophages and DCs, either untreated or treated with exogenous rIFN-γ (R&D Systems), was analyzed using a FACSCalibur flow cytometer. Dead cells were eliminated from the analysis by staining with propidium iodide (Sigma Chemical Co., St. Louis, MO), and 1×10^4 live cells were analyzed. For the analysis of cell surface antigens, the following mAbs were used: fluorescein isothiocyanate (FITC)-conjugated mAbs against HLA-ABC (G46-2.6), HLA-DR (L243), CD14 (M5E2), CD40 (5C3) and CD86 (FUN-1). These mAbs were obtained from BD PharMingen (San Diego, CA).

APC function of rBCG-infected macrophages and DCs

The ability of rBCG-infected macrophages to stimulate T cells was assessed using an autologous mixed-lymphocyte assay as previously described (Wakamatsu *et al.*, 1999; Hashimoto *et al.*, 2002). The responder $CD4^+$ T cells were purified from freshly thawed PBMCs by using a CD4-negative isolation kit (Dynabeads 450; Dynal) (Wakamatsu *et al.*, 1999). The purity of $CD4^+$ T cells was more than 95% as assessed by fluorescence-activated cell sorting (FACS) analysis. Naïve $CD4^+$ T cells were produced by further treatment of $CD4^+$ T cells with an mAb to CD45RO antigen, followed by incubation with beads coated with goat antimouse IgG. Memory-type T cells were similarly produced by the treatment of cells with an mAb to CD45RA antigen. The purified responder cells (1×10^5 well^{-1}) were plated in 96-well round-bottom tissue culture plates and macrophages or DCs were added to give the indicated APC/$CD4^+$ T-cell ratio. Supernatants of the cocultures were collected on day 4 and the concentration of cytokines was determined. In some cases, macrophages were treated with the indicated dose of exogenous rGM-CSF (Pepro Tech) in advance of infection with rBCGs. Further, macrophages were infected with rBCGs in the presence of neutralizing mAb to IL-10 (JES3-9D7; Rat IgG, BD PharMingen) or control normal rat IgG. Macrophages infected with BCGs were further costimulated with either rCD40L (Pepro Tech) or rIFN-γ (R&D Systems), and in some cases, the macrophages were stimulated with rIFN-γ in the presence of anti-IFN-γ receptor α chain (CD119) (GIR-208, mouse IgG1, BD PharMingen) or control normal mouse IgG. In other cases, macrophages infected with BCG-ΔUT in the presence of exogenous rIFN-γ were treated with either mAb to HLA-DR (L243, mouse IgG2a), CD86 (IT2.2, mouse IgG2b, BD PharMingen) or control normal mouse IgG, and subsequently cocultured with responder $CD4^+$ T cells. The concentration of IFN-γ produced by $CD4^+$ T cells was quantified using an enzyme assay kit [OptEIA Human enzyme linked immunosorbent assay (ELISA) Set; BD Biosciences].

Production of IL-12p70 and IL-1β by DCs

The ability of DCs to produce IL-12p70 and IL-1β on stimulation with BCG-Tokyo or BCG-ΔUT was assessed. The DCs were stimulated with BCGs at the indicated MOI for 24 h, and the concentration of these cytokines was quantified using the Opt EIA Human ELISA Set.

Animal studies

For inoculation into mice, BCG-Tokyo and BCG-ΔUT were cultured in Middlebrook 7H9 to log phase and stored at 10^8 CFU mL^{-1} at −80 °C. Before aliquots were used for inoculation, the concentration of viable bacilli was determined by plating cells on the Middlebrook 7H10 agar plate. Three 5-week-old C57BL/6J mice per group were inoculated intradermally with 0.1 mL phosphate-buffered saline (PBS) containing 1×10^2 or 1×10^3 BCG-Tokyo or BCG-ΔUT. The animals were kept under specific pathogen-free conditions and were supplied with sterilized food and water. Four weeks after injection, the spleens were removed, and the splenocytes were suspended at a concentration of 2×10^6 cells mL^{-1} in culture medium, and stimulated with the indicated concentration of BCC or MLM in triplicate in 96-well round-bottomed microplates. The individual culture supernatants were collected 3 days after stimulation, and IFN-γ and IL-2 were measured using an OptEIA mouse ELISA set.

Statistical analysis

The Student's *t*-test was applied to determine statistical differences.

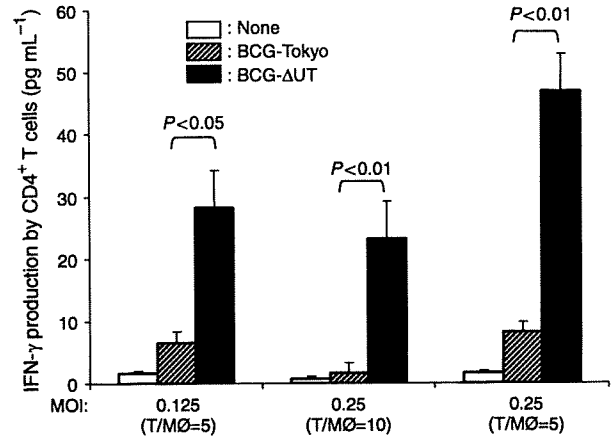

Fig. 2. Production of IFN-γ by CD4+ T cells. Macrophages, differentiated by 5 days of culture with rM-CSF from monocytes, were infected with BCG-Tokyo (parental BCG) or BCG-ΔUT at the indicated MOI, and cultured for another 2 days in the presence of rM-CSF. These macrophages were used as a stimulator of autologous CD4+ T cells (1×10^5 cells well^{-1}) at the indicated T-cell/macrophage ratio in a 4-day culture. A representative example of three separate experiments is shown. Assays were performed in triplicate and the results are expressed as the means ± SD. Titers were statistically compared using Student's *t*-test.

Results

Induction of the fusion of BCG-ΔUT-infected phagosomes with lysosomes

The efficacy with which BCG-ΔUT-infected phagosomes fused with lysosomes in macrophages was examined using confocal microscopy. Lysosomes were stained with anti-LAMP1 mAb after treatment of THP-1 cells with FITC-labeled BCG-Tokyo or BCG-ΔUT for 24 h. The parental BCG colocalized with lysosomes less efficiently than BCG-ΔUT (data not shown). Therefore, BCG-ΔUT may at least partially enhance the ability to induce phagosomal maturation.

T-cell-stimulating activity of BCG-ΔUT

The activity of BCG-ΔUT to stimulate IFN-γ-producing CD4+ T cells, when infected to macrophages, was assessed (Fig. 2). BCG-ΔUT-infected macrophages activated unseparated CD4+ T cells to release IFN-γ substantially more efficiently than parent BCG-infected macrophages. Although BCG-ΔUT-infected macrophages also induced production of IL-2 from CD4+ T cells (data not shown), the extent of IFN-γ (< 50 pg mL^{-1}) and IL-2 production was not as high as expected. Furthermore, BCG-ΔUT did not induce the activation of naïve CD4+ T cells (data not shown). As the activation of T cells is largely influenced by the cytokine milieu, in which T cells and their stimulators are present, we determined the level of cytokines produced from macrophages on stimulation with BCG-ΔUT. BCG-ΔUT produced significantly more cytokines, such as IL-10, GM-CSF, TNFα and IL-1β, than the parental BCG (data not shown). It has been reported that IL-10 inhibits the APC-mediated activation of T cells (Granelli-Piperno *et al.*, 2004) and GM-CSF regulates the function of macrophages (Makino *et al.*, 2007). To examine the role of IL-10 on T-cell activation, macrophages were infected with BCGs in the presence of a neutralizing mAb to IL-10 (Fig. 3a). The IFN-γ production by stimulated CD4+ T cells was not influenced by the treatment of macrophages with control IgG; however, a significantly higher level of IFN-γ was produced on treatment with the neutralizing mAb to IL-10. The up-regulation by IL-10 mAb treatment was observed in both BCG-Tokyo and BCG-ΔUT in a similar fashion. Furthermore, the pretreatment of macrophages with exogenous GM-CSF also significantly upregulated the antigen-presenting function of macrophages, although the effect of GM-CSF was more pronounced in BCG-ΔUT-infected macrophages (Fig. 3b).

Next, we phenotypically assessed the effect of BCG-ΔUT on macrophages (Fig. 4a). BCG-ΔUT induced enhanced expression of both CD14 and CD40 on macrophages compared with BCG-Tokyo. Based on these results, we treated BCG-infected macrophages with CD40L to examine its role as a costimulator of macrophages (Fig. 4b). The CD40L treatment upregulated the T-cell activation by BCG-

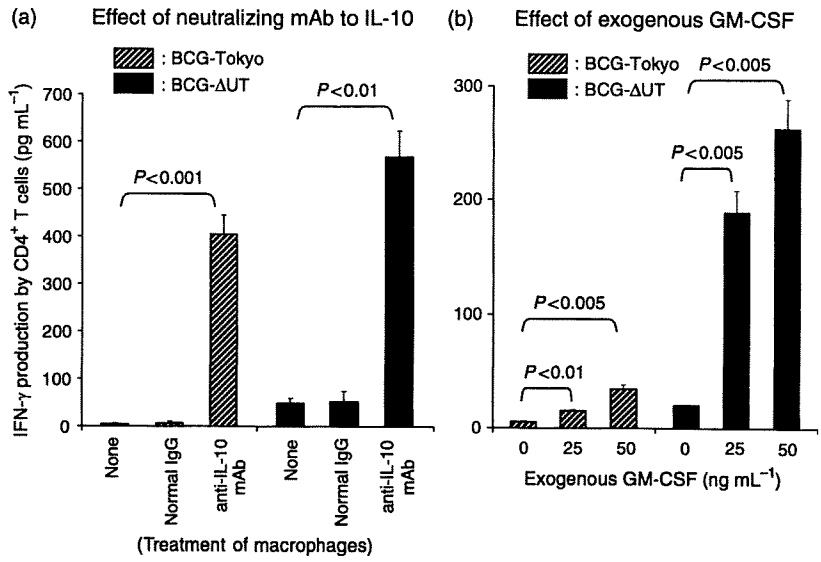

Fig. 3. Effect of IL-10 and GM-CSF on IFN-γ production. (a) Macrophages differentiated from monocytes by using rM-CSF were infected with either BCG-Tokyo or BCG-ΔUT at an MOI of 0.25 on day 5 of culture and cultured for another 2 days in the presence of rM-CSF. The BCG-infected macrophages were treated with neutralizing mAb to IL-10 or isotype-matched control IgG (10 μg mL^{-1}), and used as a stimulator of $CD4^+$ T cells, at a T-cell/macrophage ratio of 10 : 1, and cultured for another 4 days. The optimal concentration of mAb was determined in advance. (b) Macrophages obtained by 4 days of culture with rM-CSF were treated with the indicated dose of rGM-CSF. The macrophages pretreated with rGM-CSF were infected with BCG-Tokyo or BCG-ΔUT at an MOI of 0.25, cultured for another 2 days in the presence of rM-CSF used as a stimulator of $CD4^+$ T cells on day 8, at a T-cell/macrophage ratio of 10 : 1 (4 days of stimulation). A representative example of three separate experiments is shown. Assays were performed in triplicate and the results are expressed as the means ± SD. Titers were statistically compared using Student's *t*-test.

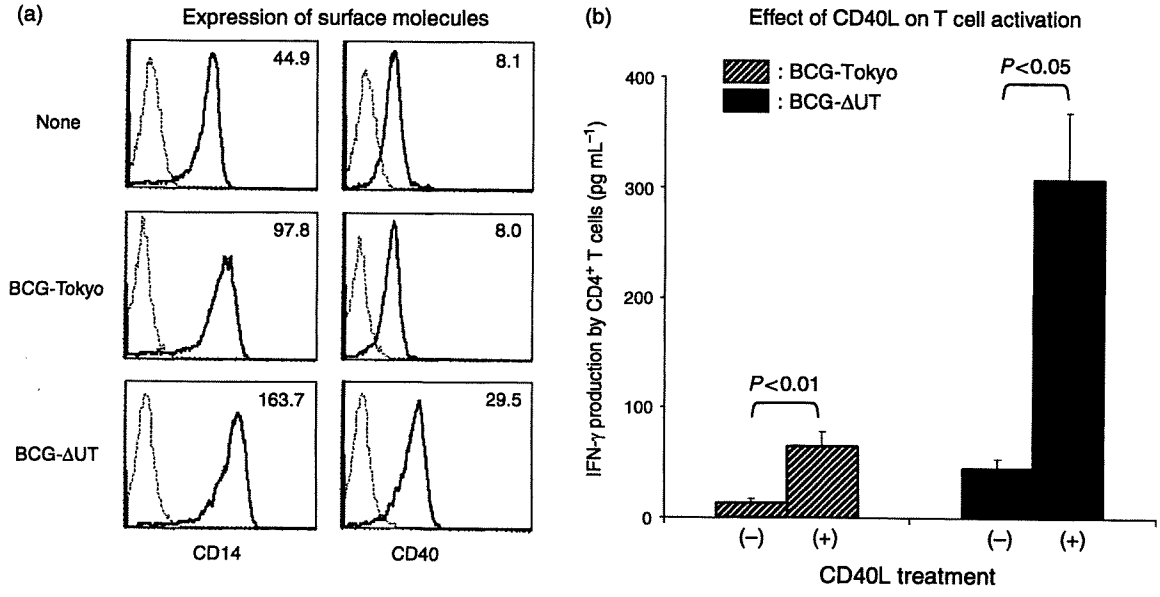

Fig. 4. (a) Expression of CD14 and CD40 molecules on macrophages. Macrophages produced by using rM-CSF were infected with BCGs at an MOI of 0.25, and cultured for another 2 days in the presence of rM-CSF. The macrophages on day 7 of culture were gated and analyzed. Dotted lines, isotype-matched control IgG; solid lines, the indicated test mAb. The number in the top right-hand corner of each panel represents the difference in mean fluorescence intensity between the control IgG and the test mAb. Representative results of three separate experiments are shown. (b) IFN-γ production by $CD4^+$ T cells stimulated with BCG-infected macrophages. Macrophages differentiated from monocytes using rM-CSF were infected with BCGs at an MOI of 0.25 on day 5 of culture, further treated with CD40L (1 μg mL^{-1}) on day 6, and used as a stimulator of $CD4^+$ T cells (T-cell/macrophage ratio of 10 : 1, 4 days of stimulation). A representative of three separate experiments is shown. Assays were performed in triplicate and the results are expressed as the means ± SD. Titers were statistically compared using Student's *t*-test.

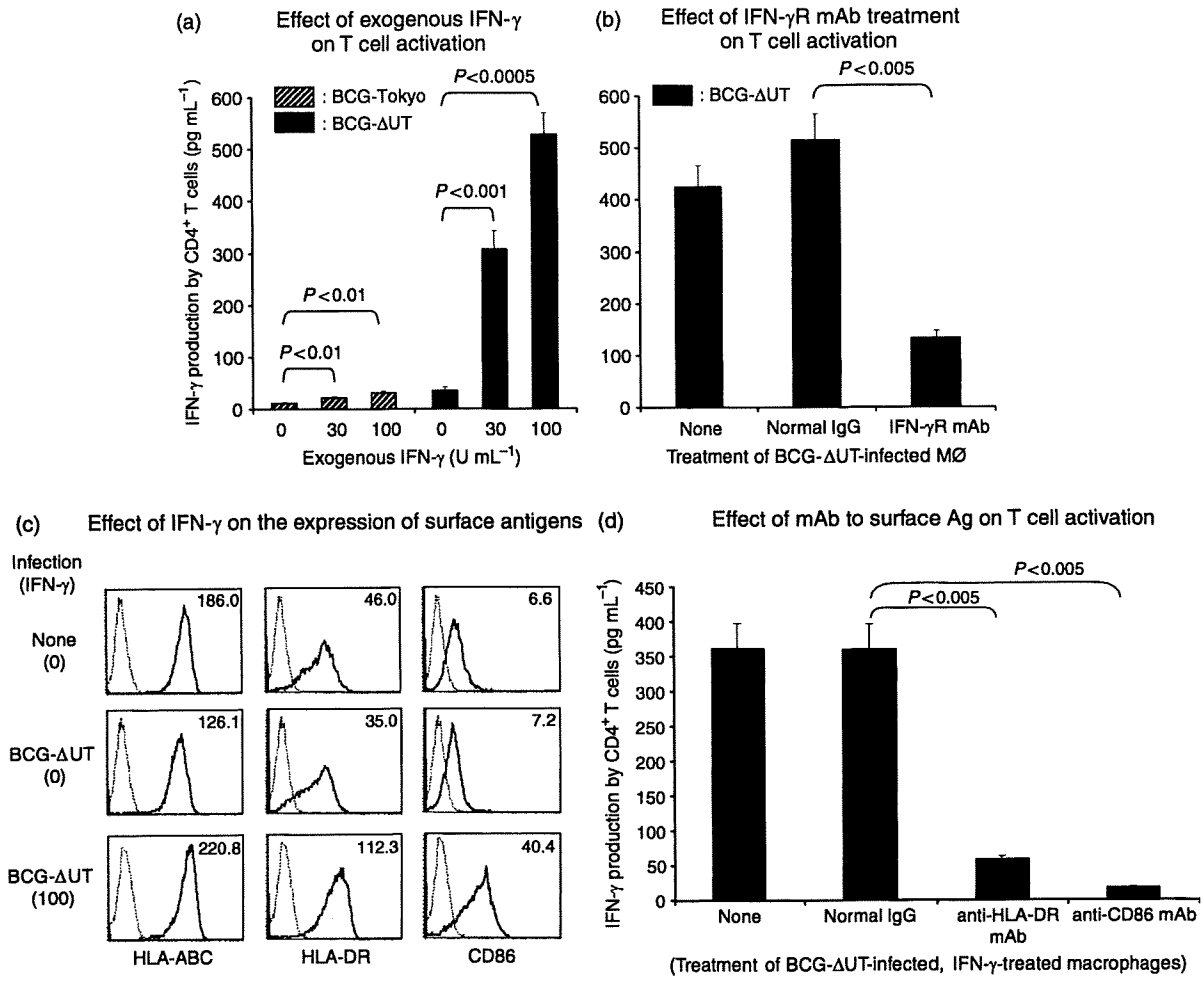

Fig. 5. (a) Effect of exogenous IFN-γ on CD4+ T-cell activation. Macrophages produced by 5 days of culture with rM-CSF from monocytes were infected with BCGs at an MOI of 0.25 and simultaneously treated with the indicated dose of exogenous IFN-γ. The macrophages were used as a stimulator of CD4+ T cells (T-cell/macrophage ratio of 10 : 1, 4 days of stimulation). A representative of three separate experiments is shown. Assays were performed in triplicate and the results are expressed as the means ± SD. Titers were statistically compared using Student's *t*-test. (b) Involvement of IFN-γ receptor in T-cell activation. Macrophages produced as in (a) were infected with BCG-ΔUT (MOI of 0.25), stimulated with exogenous IFN-γ (100 U mL^{-1}) in the presence of mAb to IFN-γ receptor α-chain (CD119) or isotype matched control IgG (10 μg mL^{-1}), and cultured for another 2 days in the presence of rM-CSF. The macrophages were used as a stimulator of CD4+ T cells (T-cell/macrophage ratio of 10 : 1, 4 days of stimulation). A representative of three separate experiments is shown. Assays were performed in triplicate and the results are expressed as the means ± SD. Titers were statistically compared using Student's *t*-test. (c) Surface expression of various molecules on BCG-ΔUT-infected, IFN-γ-treated macrophages. Macrophages produced as in (a) were infected with BCG-ΔUT (MOI of 0.25), stimulated with exogenous IFN-γ (100 U mL^{-1}) and cultured for another 2 days in the presence of rM-CSF. The macrophages on day 7 of culture were gated and analyzed. Dotted lines, isotype-matched control IgG; solid lines, the indicated test mAb. The number in the top right-hand corner of each panel represents the difference in mean fluorescence intensity between the control IgG and the test mAb. Representative results of three separate experiments are shown. (d) Involvement of surface antigens of BCG-ΔUT-infected, IFN-γ-stimulated macrophages in T-cell activation. Macrophages produced as in (a) were infected with BCG-ΔUT (MOI of 0.25), treated with exogenous IFN-γ (100 U mL^{-1}) and cultured for another 2 days in the presence of rM-CSF. These macrophages were cocultured with autologous CD4+ T cells at a T-cell/macrophage ratio of 10 : 1 in a 4-day culture in the presence of the indicated mAb (10 μg mL^{-1}). A representative of three separate experiments is shown. Assays were performed in triplicate and the results are expressed as the means ± SD. Titers were statistically compared using Student's *t*-test.

infected macrophages, but it more efficiently affected BCG-ΔUT-infected macrophages. Similarly, there was a significant difference between parent BCG and BCG-ΔUT in sensitivity to IFN-γ (Fig. 5a). However, other cytokines such as TNFα and IL-1β did not enhance the T-cell-stimulating activity of rBCG-infected macrophages. The IFN-γ treatment was effective against both BCG-Tokyo- and BCG-ΔUT-infected macrophages; however, more than a 10-fold increase in the production of IFN-γ from T cells was achieved only when BCG-ΔUT-infected macrophages

were stimulated with exogenous IFN-γ. The optimal stimulation of T cells induced the production of more than 500 pg mL^{-1} IFN-γ. The exogenous IFN-γ seems to contribute directly to the enhancement of APC function, as the IFN-γ-mediated enhancement was cancelled out by the pretreatment of BCG-ΔUT-infected macrophages with mAb to IFN-γ receptor α-chain (Fig. 5b). Furthermore, IFN-γ significantly enhanced the expression of HLA-DR and CD86 on BCG-ΔUT-infected macrophages (Fig. 5c), while the phenotypic alteration of BCG-Tokyo-infected macrophages by IFN-γ was minimum (data not shown). When BCG-ΔUT-infected, IFN-γ-treated macrophages were treated with mAb to either HLA-DR or CD86 in advance of being cocultured with CD4$^+$ T cells, IFN-γ production by the T cells was significantly inhibited, while normal murine IgG treatment did not have any effect (Fig. 5d).

CD4$^+$ T-cell activation by BCG-ΔUT-infected DCs

As BCG-ΔUT significantly but less efficiently activated CD4$^+$ T cells through macrophages in the absence of costimulation, the potency of BCG-ΔUT-infected DCs as a T-cell activator was evaluated. Expression of surface molecules on DCs infected with either BCG-Tokyo or BCG-ΔUT was examined (Fig. 6a). Expression of HLA-ABC, HLA-DR, CD86 and CD83 was more significantly upregulated by the infection with BCG-ΔUT than with BCG-Tokyo. Higher levels of IL-12p70 and IL-1β were produced by BCG-ΔUT stimulation (Fig. 6b). Furthermore, we assessed whether BCG-ΔUT activated naïve and memory CD4$^+$ T cells through DCs by using various MOI titers and multiple T/DC ratios (Fig. 6c). IFN-γ levels were significantly higher following stimulation with BCG-ΔUT than with parent BCG in both naïve and memory CD4$^+$ T cells. Also, a higher level of CD40L was expressed on CD4$^+$ T cells after stimulation with BCG-ΔUT-infected DCs (data not shown). These results indicate that the infection of DCs with BCG-ΔUT alone was sufficient, as compared with macrophages which required costimulators to drive a strong T-cell response.

Memory T-cell production by BCG-ΔUT

Another important aspect of using BCG as a vaccine is the production of memory T cells *in vivo*. We examined the response of splenic T cells obtained from BCG-infected C57BL/6 mice to mycobacterial recall antigen (Fig. 7). We used BCC as a recall antigen. At 4 weeks following infection, splenic T cells from BCG-ΔUT-infected mice produced more IFN-γ than those from mice infected with BCG-Tokyo by responding to BCC. The lymphocyte population producing IFN-γ was found to be CD4$^+$ T cells by intracellular staining (data not shown). Furthermore, upon stimulation with MLM, which contains immunodominant antigens of *M. leprae*, CD4$^+$ T cells from BCG-ΔUT-infected mice produced significantly higher levels of IFN-γ than those from uninfected or BCG-Tokyo-infected mice (Fig. 7).

Discussion

To date, BCG is the only suitable vaccine against leprosy; however, its efficacy is quite limited. Overall efficacy in one meta-analysis was reported to be only 26% (Setia *et al.*, 2006). Several reasons might explain why BCG cannot block multiplication of *M. leprae* or inhibit the development of leprosy. The most important defect of BCG is that it is retained in phagosomes of macrophages, avoiding phagosomal acidification and hence interfering in the efficient fusion of BCG-containing phagosomes with lysosomes (Clements *et al.*, 1995; Reyrat *et al.*, 1995; Grode *et al.*, 2005). The lack of phagosome–lysosome fusion inhibits the trafficking of BCG-derived antigens through the major histocompatibility class (MHC) II pathway, which is enrolled for preferential stimulation of CD4$^+$ T cells, the most important cells involved in inhibition of *M. leprae* growth (Sendide *et al.*, 2004). Further, macrophages produce abundant amounts of IL-10 on infection with BCG, which, in turn, inhibits the activation of CD4$^+$ T cells (Mochida-Nishimura *et al.*, 2001; Granelli-Piperno *et al.*, 2004).

In the present study, we constructed a recombinant BCG (BCG-ΔUT) that lacks a *urease* gene through allelic exchange of chromosomal DNA. As urease is involved in the maintenance of intraphagosomal pH at neutral (Grode *et al.*, 2005) or slightly alkaline values (Sendide *et al.*, 2004), lack of this enzyme may contribute to the induction of phagosomal acidification (Sendide *et al.*, 2004), thereby promoting the fusion of BCG-containing phagosomes with lysosomes. The efficient colocalization of BCG-ΔUT with lysosome was observed, leading us to expect an efficient enhancement of T-cell activation by BCG-ΔUT-infected macrophages. Previously, rBCG deficient in urease C was produced by a similar system and found to be superior to parental BCG in producing acidic conditions (pH 4.5–5.5) in BCG-infected phagosomes in murine macrophages (Reyrat *et al.*, 1995; Grode *et al.*, 2005). However, it was not demonstrated whether the rBCG deficient in urease C promoted the MHC class II trafficking pathway and actually activated human CD4$^+$ T cells through APCs. The newly constructed BCG-ΔUT lacked urease activity and *in vitro* studies confirmed that it could not degrade urea to ammonia. When BCG-ΔUT was infected to macrophages, it activated human CD4$^+$ T cells more efficiently than the parental BCG. However, the amount of IFN-γ released from the T cells was not as high as expected (< 50 pg mL^{-1}). These results suggest that

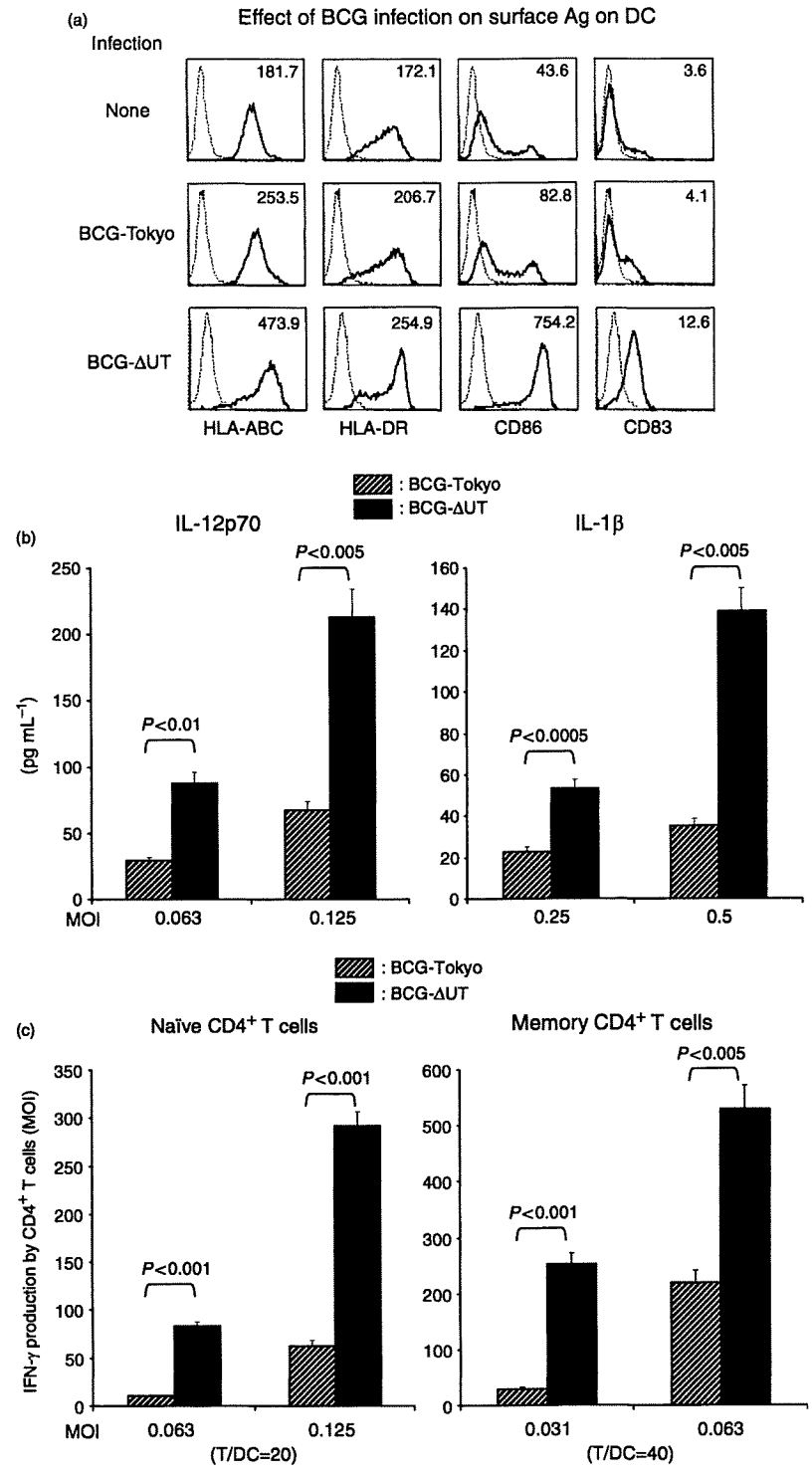

Fig. 6. (a) Expression of various molecules on BCG-infected DCs. Monocyte-derived immature DCs were infected with either BCG-Tokyo or BCG-ΔUT at an MOI of 0.25 and cultured for another 2 days in the presence of rGM-CSF and rIL-4. The DCs from day 5 were gated and analyzed. Dotted lines, isotype-matched control IgG; solid lines, the indicated test mAb. The number in the top right-hand corner of each panel represents the difference in mean fluorescence intensity between the control IgG and the test mAb. Representative results of three separate experiments are shown. (b) Cytokine production from DCs stimulated by BCG. Monocyte-derived DCs from 4 days of culture in the presence of rGM-CSF and rIL-4 were stimulated with the indicated dose of either BCG-Tokyo or BCG-ΔUT for 24 h. The concentration of the indicated cytokine was determined by the ELISA method. A representative of three separate experiments is shown. Assays were performed in triplicate and the results are expressed as the means ± SD. Titers were statistically compared using Student's *t*-test. (c) IFN-γ production by naïve $CD4^+$ T cells and memory $CD4^+$ T cells. DCs obtained from monocytes infected with either BCG-Tokyo or BCG-ΔUT were used as a stimulator of naïve and memory $CD4^+$ T cells in a 4-day culture. A representative of three separate experiments is shown. Assays were performed in triplicate and the results are expressed as the means ± SD. Titers were statistically compared using Student's *t*-test.

improvement of intraphagosomal pH milieu for efficient phagosome–lysosome fusion was not sufficient for the induction of full T-cell activation as far as macrophages were concerned. Thus, we further searched for factors which might be helpful in inducing full activation of T cells. First, we examined the influence of endogenously produced IL-10, as abundant IL-10 was produced from macrophages by infection with BCG-ΔUT (data not shown). The neutralization of IL-10 from macrophages drastically enhanced T-cell activation (Fig. 3a). Furthermore, pretreatment of